Configurational Control of Low-Symmetry Heteroleptic Metal-Organic Cages with Asymmetric Ligands

Hao Yu,[1] Ziteng Guo,[1] Jie Tang,[1] Ningxu Han,[1] Junjuan Shi,[1] Meng Li,[1] Houyu Zhang[1] and Ming Wang[1,*]

[1]State Key Laboratory of Supramolecular Structure and Materials, College of Chemistry, Jilin University, Changchun, Jilin 130012, China

Table of Contents

1. Materials and Methods

General procedure. The reagents were commercially available from Sigma-Aldrich, Acros, Aladdin and used without further purification. Column chromatography was conducted using SiO_2 (Qingdao ocean column chromatography silica gel, 200-300 mesh) and the separated products were visualized by UV light. NMR spectra data were recorded on Bruker Avance 500-MHz, 600-MHz NMR and Qone AS 400-MHz NMR spectrometer in $CDCl_3$, DMSO-d_6, and DMF-d_7. ESI-MS data was recorded with a Q Exactive mass spectrometer for ligands and a Waters Synapt G2 tandem mass spectrometer for complexes. The simulations of the molecular structures of $\mathbf{Pd_3L^B_6}$, $\mathbf{Pd_4L^B_8}$ and ***trans*-$\mathbf{Pd_{12}L^C_{24}}$** were performed on Materials Studio version 8.0 and optimized using two modes: Geometry Optimization tasks and Anneal Optimization tasks.

2. Synthesis of Ligands and Complexes

2.1 Synthesis of the ligand L^A and cage $Pd_{12}L^A_{24}$

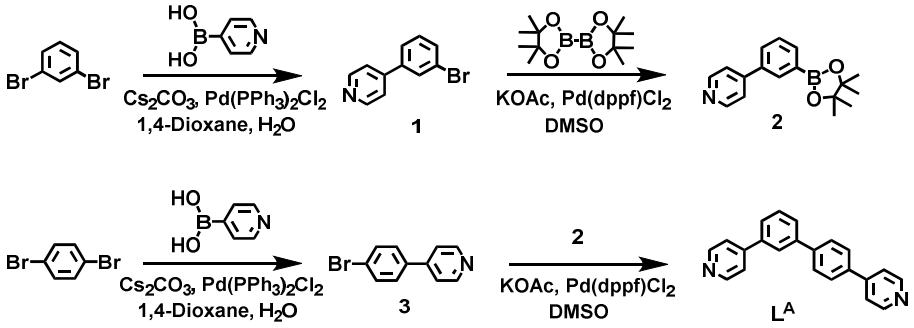

Scheme S1. Synthetic routes of ligand $\mathbf{L^A}$.

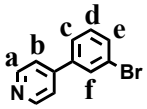

2.1.1 Synthesis of compound **1**. 1,3-dibromobenzene (5.000 g, 21.4 mmol), pyridin-4-ylboronic acid (1.096 g, 8.91 mmol), Cs_2CO_3 (2.900 g, 8.91 mmol) and $Pd(PPh_3)_2Cl_2$ (0.312 g, 0.445 mmol) were added to a 200 mL Schlenk flask. The reaction vessel was evacuated under vacuum and flushed with N_2 for three times, then 100 mL 1,4-dioxane and 25 mL ultrapure water were injected. The reaction was reacted at 88 °C for 12 h. After cooling to room temperature, the mixture was extracted with dichloromethane. The combined organic layer was concentrated in vacuo, and then the crude product was purified by flash column chromatography with dichloromethane: ethanol (100:2.0, v/v) to obtain the compound **1** (1.494 g, 72%). ^{1}H NMR (400 MHz, $CDCl_3$, 300 K) δ (ppm): 8.72 – 8.63 (m, 2H, Ph-H^a), 7.77 (t, J = 1.9 Hz, 1H, Ph-H^f), 7.56 (dddd, J = 6.7, 5.7, 1.9, 1.0 Hz, 2H, Ph-$H^{c,e}$), 7.49 – 7.44 (m, 2H, Ph-H^b), 7.36 (t, J = 7.9 Hz, 1H, Ph-H^d). ^{13}C NMR (100 MHz, $CDCl_3$, 300 K) δ (ppm): 150.20, 146.53, 139.98, 131.79, 130.47, 129.84, 125.43, 123.05, 121.32.

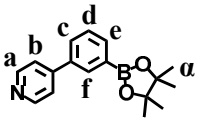

2.1.2 Synthesis of compound **2**. A mixture of compound **1** (0.692 g, 2.971 mmol), pinacol diborate (0.755 g, 2.971 mmol), KOAc (1.746 g, 17.82 mmol) and $Pd(dppf)Cl_2$ (0.109 g, 0.149 mmol) was added to a 100 mL Schlenk flask. The reaction vessel was evacuated under vacuum and flushed with N_2 for three times, then 40 mL DMSO was injected. The mixture was reacted at 80 °C for 16 h. After cooling to room temperature, the reactant was extracted with dichloromethane. The combined organic layer was concentrated in vacuo, and then the crude product was purified by flash column chromatography with dichloromethane: ethanol (100:2.0, v/v) to obtain the compound **2** (0.651 g, 78%). ^{1}H NMR (400 MHz, $CDCl_3$, 300 K) δ (ppm): 8.66 – 8.61 (m, 2H, Ph-H^a), 8.08 (t, J = 1.6 Hz, 1H, Ph-H^f), 7.88 (dt, J = 7.3, 1.2 Hz, 1H, Ph-H^e), 7.72 (ddd, J = 7.8, 2.1, 1.3 Hz, 1H, Ph-H^c), 7.57 – 7.54 (m, 2H, Ph-H^b), 7.49 (t, J = 7.7 Hz, 1H, Ph-H^d), 1.36 (s, 12H, Ph-$H^α$). ^{13}C NMR (100 MHz, $CDCl_3$, 300 K) δ (ppm): 150.01, 148.62, 137.44, 135.58, 133.42, 132.25, 129.84, 128.62, 121.90, 84.18, 24.99.

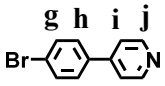

2.1.3 Synthesis of compound **3**. 4-pyridineboronic acid (0.440 g, 3.575 mmol), 1,4-dibromobenzene (2.000 g, 8.58 mmol), Cs_2CO_3 (1.160 g, 3.575 mmol) and $Pd(PPh_3)_2Cl_2$ (0.130 g, 0.179 mmol) were added to a 100 mL Schlenk flask. The reaction vessel was evacuated under vacuum and flushed with N_2 for three times, then 48 mL 1,4-dioxane and 12 mL ultrapure water were injected. The reaction was reacted at 88 °C for 10 h. After cooling to room temperature, the mixture was extracted with dichloromethane. The combined organic layer was concentrated in vacuo, and then the crude product was purified by flash column chromatography with dichloromethane: ethanol (100:2.0, v/v) to obtain the compound **3** (0.566 g, 68%). ^{1}H NMR (400 MHz, $CDCl_3$, 300 K) δ (ppm): 8.71 – 8.64 (m, 2H, Ph-H^j), 7.63 (d, J = 8.4 Hz, 2H, Ph-H^g), 7.54 – 7.49 (m, 2H, Ph-H^h), 7.49 – 7.44 (m, 2H, Ph-H^i). ^{13}C NMR (100 MHz, $CDCl_3$, 300 K) δ 150.52, 147.20, 137.13, 132.40, 128.64, 123.65, 121.44.

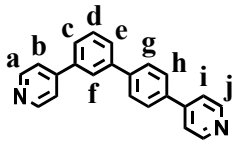

2.1.4 Synthesis of ligand $\mathbf{L^A}$. A mixture of compound **2** (0.395 g, 1.404 mmol), compound **3** (0.327 g, 1.404 mmol), KOAc (0.826 g, 8.43 mmol) and $Pd(dppf)Cl_2$ (0.052 g, 0.07 mmol) was added to a 100 mL Schlenk flask. The Schlenk bottle was evacuated under vacuum and flushed with N_2 for three times, and then 40 mL DMSO was added. The mixture was reacted at 80 °C for 16 hours. After cooling to room temperature, the mixture was extracted with dichloromethane. After removal of solvent under vacuum, the mixture was purified by column chromatography on silica gel with dichloromethane: ethanol (100:3, v/v) as eluent to obtain the ligand $\mathbf{L^A}$ (0.264 g, 61%). ^{1}H NMR (500 MHz, $CDCl_3$, 300 K) δ (ppm): 8.70 (dt, J = 6.0, 2.8 Hz, 4H, Ph-$H^{a,j}$), 7.88 (t, J = 1.8 Hz, 1H, Ph-H^f), 7.77 (s, 4H, Ph-$H^{g,h}$), 7.72 (dd, J = 7.6, 1.6 Hz, 1H, Ph-H^e), 7.66 (dd, J = 7.8, 1.6 Hz, 1H, Ph-H^e), 7.63 – 7.55 (m, 5H, Ph-$H^{d,b,i}$). ^{13}C NMR (125 MHz, $CDCl_3$, 300 K) δ (ppm): 150.47, 148.32, 147.81, 141.51, 141.39, 139.09, 137.54, 129.87, 128.06, 127.91, 127.67, 126.51, 125.97, 121.89, 121.61. ESI-MS (*m/z*): Calcd. for $[C_{22}H_{16}N_2+H]^+$: 309.13. Found: 309.13.

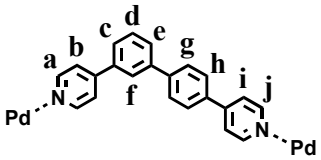

2.1.5 Synthesis of cage $\mathbf{Pd_{12}L^A_{24}}$. Accurately added ligand $\mathbf{L^A}$ (0.0062 g, 0.02 mmol) and $Pd(CH_3CN)_4(BF_4)_2$ (0.0044 g, 0.01 mmol), and dissolve them in 1 mL DMSO. The mixture was heated to 70 °C for 8 h. After the assembly was completed, the assembly solution was dropped into 8 mL of ether. After standing for ten minutes, the precipitated solid was centrifuged and washed twice with ether. Finally, a white solid was obtained (0.0082 g, 91%). ^{1}H NMR (500 MHz, DMSO-d_6, 300 K) δ (ppm): 9.36 (s, 4H, Ph-$H^{a,j}$), 8.26 (d, J = 79.0 Hz, 5H, Ph-$H^{b,f,h}$), 7.99 (s, 6H, Ph-$H^{c,e,g,i}$), 7.64 (s, 1H, Ph-H^d). ^{13}C NMR (125 MHz, DMSO-d_6, 300 K) δ (ppm): 151.10, 149.73, 141.14, 139.50, 134.70, 133.70, 130.30, 129.22, 127.80, 124.05. ESI-MS (*m/z*): 1257.76 $[M\text{-}8BF_4^-]^{8+}$ (calcd *m/z*: 1257.76), 1108.32 $[M\text{-}9BF_4^-]^{9+}$ (calcd *m/z*: 1108.32), 988.90 $[M\text{-}10BF_4^-]^{10+}$ (calcd *m/z*: 988.90), 891.01 $[M\text{-}11BF_4^-]^{11+}$ (calcd *m/z*: 891.01), 809.57 $[M\text{-}12BF_4^-]^{12+}$ (calcd *m/z*: 809.57).

2.2 Synthesis of the ligand $\mathbf{L^B}$ and complexes of $\mathbf{Pd_4L^B_8}$ and $\mathbf{Pd_3L^B_6}$

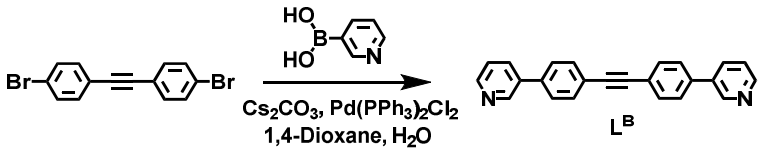

Scheme S2. The synthetic route of ligand $\mathbf{L^B}$.

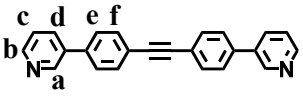

2.2.1 Synthesis of ligand $\mathbf{L^B}$. A mixture of 1,2-bis(4-bromophenyl)ethyne (0.500 g, 1.497 mmol), pyridin-3-ylboronic acid (0.516 g, 4.193 mmol), Cs_2CO_3(0.976 g, 2.995 mmol) and $Pd(PPh_3)_2Cl_2$ (0.105 g, 0.149 mmol) was added to a 100 mL Schlenk flask. The Schlenk bottle was evacuated under vacuum and flushed with N_2 for three times, and then 40 mL 1,4-dioxane and 10 mL ultrapure water were added. The mixture was reacted at 88 °C for 2 days. After cooling to room temperature, the mixture was extracted with dichloromethane. After removal of solvent under vacuum, the residue was purified by column chromatography on silica gel with dichloromethane: ethanol (100:3, v/v) as eluent to obtain the ligand $\mathbf{L^B}$ (0.363 g, 73%). ^{1}H NMR (500 MHz, $CDCl_3$, 300 K) δ (ppm): 8.88 (s, 1H, Ph-H^a), 8.64 – 8.60 (m, 1H, Ph-H^b), 7.90 (dt, J = 8.0, 1.9 Hz, 1H, Ph-H^d), 7.66 (d, J = 8.1 Hz, 2H, Ph-H^e), 7.60 (d, J = 8.1 Hz, 2H, Ph-H^f), 7.38 (dd, J = 7.9, 4.8 Hz, 1H, Ph-H^c). ^{13}C NMR (125 MHz, $CDCl_3$, 300 K) δ (ppm): 148.95, 148.32, 137.84, 135.97, 134.36, 132.48, 127.21, 123.78, 123.14, 90.32. ESI-MS (*m/z*): Calcd. for $[C_{24}H_{16}N_2+H]^+$: 333.13. Found: 333.13.

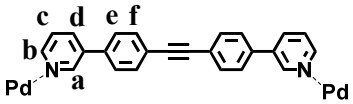

2.2.2 Synthesis of complexes of $\mathbf{Pd_4L^B_8}$ and $\mathbf{Pd_3L^B_6}$. Accurately added ligand $\mathbf{L^B}$ (0.0033 g, 0.01 mmol) and $Pd(CH_3CN)_4(BF_4)_2$ (0.0022 g, 0.005 mmol), and dissolve them in 0.5 mL DMF-d_7. The mixture was heated at 70 °C for 8 h. Finally, a mixture of $\mathbf{Pd_4L^B_8}$ and $\mathbf{Pd_3L^B_6}$ was obtained. ^{1}H NMR (500 MHz, DMF-d_7, 300 K) δ (ppm): 10.38 (d, J = 2.3 Hz, Ph-H^a), 10.29 (s, Ph-$H^{a''}$), 10.04 – 9.99 (m, Ph-$H^{b'}$), 9.95 (d, J = 2.1 Hz, Ph-$H^{a'}$), 9.78 (d, J = 5.7 Hz, Ph-$H^{b''}$), 9.54 – 9.49 (m, Ph-H^b), 8.76 (dt, J = 8.3, 1.6 Hz, Ph-$H^{d'}$), 8.75 – 8.72 (m, Ph-$H^{d''}$), 8.67 (dt, J = 8.3, 1.6 Hz, Ph-H^d), 8.24 (dd, J = 8.2, 5.6 Hz, Ph-$H^{c'}$), 8.18 – 8.11 (Ph-$H^{e',c''}$), 8.11 – 8.04 (Ph-$H^{e'',e}$), 8.01 – 7.95 (Ph-$H^{f'',c,\ f,\ f'}$). ^{13}C NMR (125 MHz, DMF-d_7, 300 K) δ (ppm): 150.72, 150.37, 149.99, 149.40, 149.10, 139.23, 138.84, 138.78, 138.57, 135.22, 135.14, 132.78, 132.63, 128.19, 127.92, 127.81, 127.74, 127.63, 124.02, 123.90, 117.82, 90.90, 90.77, 90.61, 56.88. ESI-MS of $\mathbf{Pd_4L^B_8}$ (*m/z*): 453.51 $[M\text{-}7BF_4^-]^{7+}$ (calcd *m/z*: 453.51), 543.43 $[M\text{-}6BF_4^-]^{6+}$ (calcd *m/z*: 543.43), 669.55 $[M\text{-}5BF_4^-]^{5+}$ (calcd *m/z*: 669.55), 858.47 $[M\text{-}4BF_4^-]^{4+}$ (calcd *m/z*: 858.47), 1173.21 $[M\text{-}3BF_4^-]^{3+}$ (calcd *m/z*: 1173.21); ESI-MS of $\mathbf{Pd_3L^B_6}$ (*m/z*): 480.52 $[M\text{-}5BF_4^-]^{5+}$ (calcd *m/z*: 480.52), 622.14 $[M\text{-}4BF_4^-]^{4+}$ (calcd *m/z*: 622.14), 858.42 $[M\text{-}3BF_4^-]^{3+}$ (calcd *m/z*: 858.42).

2.3 Synthesis of the ligand $\mathbf{L^C}$ and cage $\mathbf{Pd_{12}L^C_{24}}$

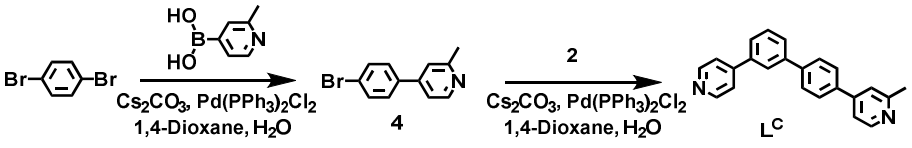

Scheme S3. Synthetic routes of ligand $\mathbf{L^C}$.

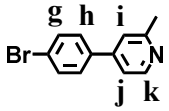

2.3.1 Synthesis of compound **4**. (2-methylpyridin-4-yl)boronic acid (0.490 g, 3.575 mmol), 1,4-dibromobenzene (2.000 g, 8.58 mmol), Cs_2CO_3 (1.160 g, 3.575 mmol) and $Pd(PPh_3)_2Cl_2$ (0.130 g, 0.179 mmol) were added to a 100 mL Schlenk flask. The reaction vessel was evacuated under vacuum and flushed with N_2 for three times, then 48 mL 1,4-dioxane and 12 mL ultrapure water were injected. The reaction was reacted at 88 °C for 10 h. After cooling to room temperature, the mixture was extracted with dichloromethane. The combined organic layer was concentrated in vacuo, and then the crude product was purified by flash column chromatography with dichloromethane: ethanol (100:2.0, v/v) to obtain the compound **4** (0.618 g, 70%). ^{1}H NMR (400 MHz, $CDCl_3$, 300 K) δ (ppm): 8.54 (d, J = 5.2 Hz, 1H, Ph-H^k), 7.63 – 7.57 (m, 2H, Ph-H^g), 7.51 – 7.46 (m, 2H, Ph-H^h), 7.33 (d, J = 1.9 Hz, 1H, Ph-H^i), 7.27 (d, J = 6.6 Hz, 1H, Ph-H^j). ^{13}C NMR (100 MHz, $CDCl_3$, 300 K) δ 159.20, 149.83, 147.69, 137.48, 132.37, 128.72, 123.51, 121.09, 118.73, 24.69.

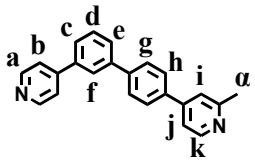

2.3.2 Synthesis of ligand $\mathbf{L^C}$. A mixture of compound **2** (0.500 g, 1.778 mmol), compound **4** (0.439 g, 1.778 mmol), Cs_2CO_3 (0.579 g, 1.778 mmol) and $Pd(PPh_3)_2Cl_2$ (0.062 g, 0.089 mmol) was added to a 100 mL Schlenk flask. The Schlenk bottle was evacuated under vacuum and flushed with N_2 for three times, and then 40 mL 1,4-dioxane and 10 mL ultrapure water were added. The mixture was reacted at 88 °C for 12 h. After cooling to room temperature, the mixture was extracted with dichloromethane. After removal of solvent under vacuum, the residue was purified by column chromatography on silica gel with dichloromethane: ethanol (100:3, v/v) as eluent to obtain the ligand $\mathbf{L^C}$ (0.355 g, 62%). ^{1}H NMR (500 MHz, $CDCl_3$, 300 K) δ (ppm): 8.71 – 8.67 (m, 2H, Ph-H^a), 8.58 (d, J = 5.2 Hz, 1H, Ph-H^k), 7.87 (t, J = 1.9 Hz, 1H, Ph-H^f), 7.75 (s, 4H, Ph-$H^{g,h}$), 7.71 (dt, J = 7.7, 1.6 Hz, 1H, Ph-H^c), 7.65 (dt, J = 7.8, 1.5 Hz, 1H, Ph-H^e), 7.60 (d, J = 7.6 Hz, 1H, Ph-H^d), 7.58 – 7.56 (m, 2H, Ph-H^b), 7.44 (d, J = 1.7 Hz, 1H, Ph-H^i), 7.38 (dd, J = 5.3, 1.8 Hz, 1H, Ph-H^j), 2.65 (s, 3H, Ph-H^α). ^{13}C NMR (125 MHz, $CDCl_3$, 300 K) δ (ppm): 158.97, 150.45, 149.57, 148.38, 141.42, 139.07, 137.74, 129.86, 127.99, 127.91, 127.70, 126.48, 125.97, 121.90, 121.26, 118.91, 24.60. ESI-MS (*m/z*): Calcd. for $[C_{23}H_{18}N_2+H]^+$: 323.15. Found: 323.15.

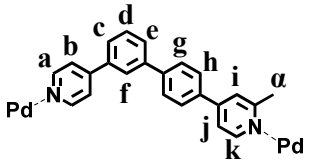

2.3.3 Synthesis of cage $\mathbf{Pd_{12}L^C_{24}}$. Accurately added ligand $\mathbf{L^C}$ (0.0064 g, 0.02 mmol) and $Pd(CH_3CN)_4(BF_4)_2$ (0.0044 g, 0.01 mmol), and dissolve them in 1 mL DMF. The mixture was heated at 70 °C for 8 h. After the assembly was completed, the assembly solution was dropped into 8 mL of ether. After standing for ten minutes, the precipitated solid was centrifuged and washed twice with ether. Finally, a light gray solid was obtained (0.0086 g, 93%). ^{1}H NMR (500 MHz, DMF-d_7, 300 K) δ (ppm): 9.8-9.2 (s, 3H, Ph-$H^{a,k}$), 8.6-7.9 (d, J = 132.5 Hz, 11H, Ph-$H^{b,c,e,f,g,h,i,j}$), 7.7 (s, 1H, Ph-H^d) , 3.69 (s, 3H, Ph-H^α). ^{13}C NMR (125 MHz, DMF-d_7, 300 K) δ (ppm): 152.21, 150.33, 141.77, 140.17, 134.02, 130.45, 129.58, 127.98, 124.53, 121.59, 117.65, 25.09. ESI-MS (*m/z*): 1497.84 $[M\text{-}7BF_4^-]^{7+}$ (calcd *m/z*: 1497.84), 1299.80 $[M\text{-}8BF_4^-]^{8+}$ (calcd *m/z*: 1299.80), 1145.76

[M-9BF_4^-]$^{9+}$ (calcd *m/z*: 1145.76), 1022.53 [M-10BF_4^-]$^{10+}$ (calcd *m/z*: 1022.53), 921.68 [M-11BF_4^-]$^{11+}$ (calcd *m/z*: 921.68), 837.52 [M-12BF_4^-]$^{12+}$ (calcd *m/z*: 837.52).

2.4 Synthesis of the cage **$Pd_6L^A{}_6L^B{}_6$** and **$Pd_6L^B{}_6L^C{}_6$**

2.4.1 Synthesis of cage **$Pd_6L^A{}_6L^B{}_6$**. Accurately added ligand **L^A** (0.0031 g, 0.01 mmol), ligand **L^B** (0.0033 g, 0.01 mmol) and $Pd(CH_3CN)_4(BF_4)_2$ (0.0044 g, 0.01 mmol), and dissolve them in 1 mL DMF. The mixture was heated at 70 °C for 8 h. After the assembly was completed, the assembly solution was dropped into 8 mL of ether. After standing for ten minutes, the precipitated solid was centrifuged and washed twice with ether. Finally, a white solid was obtained (0.0085 g, 92%). ^{1}H NMR (600 MHz, DMF-d_7, 300 K) δ (ppm): 9.7-9.4 (s, 8H, Ph-$H^{a',b',a,j}$), 8.52 (dd, *J* = 11.0, 5.3 Hz, 2H, Ph-$H^{d'}$), 8.4 (d, *J* = 6.3 Hz, 2H, Ph-H^{b}), 8.26 (m, 2H, Ph-H^{i}), 8.15 – 7.88 (m, 13H, Ph-$H^{c,e,f,g,h,e',c'}$), 7.8 (m, 4H, Ph-H^{f}), 7.65 (t, *J* = 8.4 Hz, 1H, Ph-H^{d}). ^{13}C NMR (125 MHz, DMF-d_7, 300 K) δ (ppm): 151.56, 150.49, 150.21, 149.60, 149.14, 148.92, 141.73, 140.06, 139.06, 138.63, 135.05, 133.98, 132.59, 130.45, 129.53, 127.94, 127.73, 125.30, 124.28, 123.81, 90.49. ESI-MS (*m/z*): 1294.72 [M-4BF_4^-]$^{4+}$ (calcd *m/z*: 1294.72), 1018.61 [M-5BF_4^-]$^{5+}$ (calcd *m/z*: 1018.61), 834.36 [M-6BF_4^-]$^{6+}$ (calcd *m/z*: 834.36), 702.82 [M-7BF_4^-]$^{7+}$ (calcd *m/z*: 702.82), 604.21 [M-8BF_4^-]$^{8+}$ (calcd *m/z*: 604.21), 527.53 [M-9BF_4^-]$^{9+}$ (calcd *m/z*: 527.53).

2.4.2 Synthesis of cage **$Pd_6L^B{}_6L^C{}_6$**. Accurately added ligand **L^B** (0.0033 g, 0.01 mmol), ligand **L^C** (0.0032 g, 0.01 mmol) and $Pd(CH_3CN)_4(BF_4)_2$ (0.0044 g, 0.01 mmol), and dissolve them in 1 mL DMF. The mixture was heated at 70°C for 8 h. After the assembly was completed, the assembly solution was dropped into 8 mL of ether. After standing for ten minutes, the precipitated solid was centrifuged and washed twice with ether. Finally, a white solid was obtained (0.0088 g, 94%). ^{1}H NMR (500 MHz, DMF-d_7, 300 K) δ (ppm): 9.8-9.3 (s, 7H, Ph-$H^{a',b',a,j}$), 8.7-8.4 (d, *J* = 40.9 Hz, 4H, Ph-$H^{d',b}$), 8.35-7.94 (m, *J* = 26.4 Hz, 14H, Ph-$H^{i,f,e',g,h,e,c,c'}$), 7.81 (s, 4H, Ph-H^{f}), 7.68 (s, 1H, Ph-H^{d}), 3.66 (s, 3H, Ph-H^{α}). ^{13}C NMR (125 MHz, DMF-d_7, 300 K) δ (ppm): 151.75, 151.16, 150.65, 150.26, 149.42, 141.82, 140.29, 139.25, 138.72, 135.18, 132.75, 130.62, 129.90, 128.07, 127.85, 125.16, 124.49, 123.98, 117.30, 90.64, 49.05. ESI-MS (*m/z*): 1315.76 [M-4BF_4^-]$^{4+}$ (calcd *m/z*: 1315.76), 1035.21 [M-5BF_4^-]$^{5+}$ (calcd *m/z*: 1035.21), 848.35 [M-6BF_4^-]$^{6+}$ (calcd *m/z*: 848.35), 714.83 [M-7BF_4^-]$^{7+}$ (calcd *m/z*: 714.83), 614.77 [M-8BF_4^-]$^{8+}$ (calcd *m/z*: 614.77).

3. ^{1}H NMR, ^{13}C NMR, 2D COSY NMR, 2D NOESY NMR and DOSY NMR

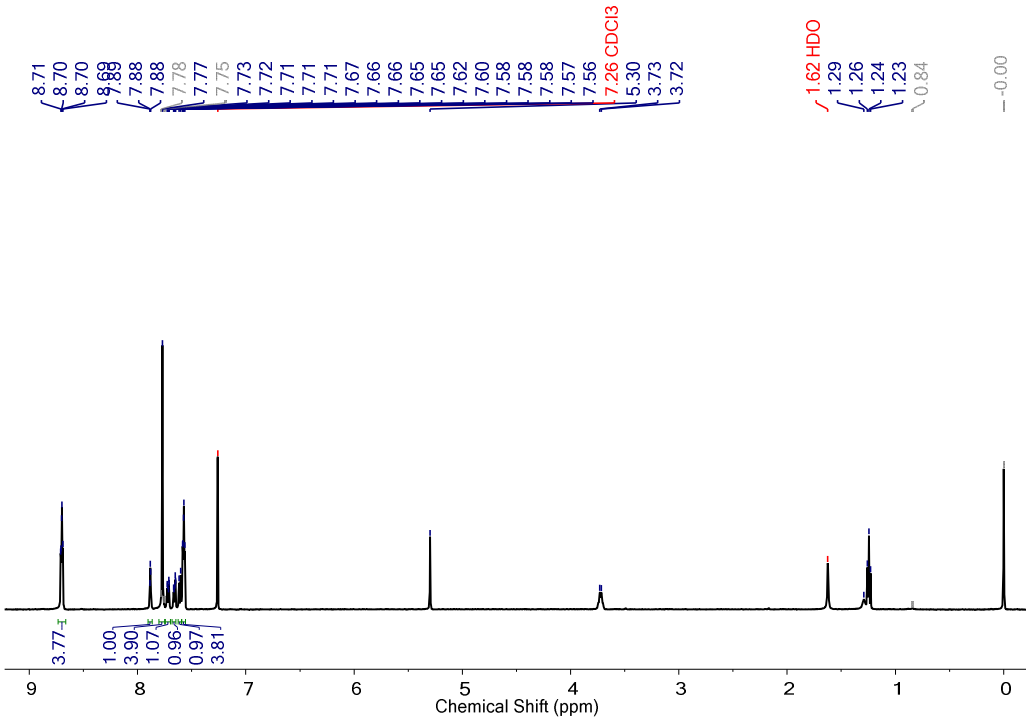

Figure S1. ^{1}H NMR (500 MHz, $CDCl_3$, 300 K) spectrum of $\mathbf{L^A}$.

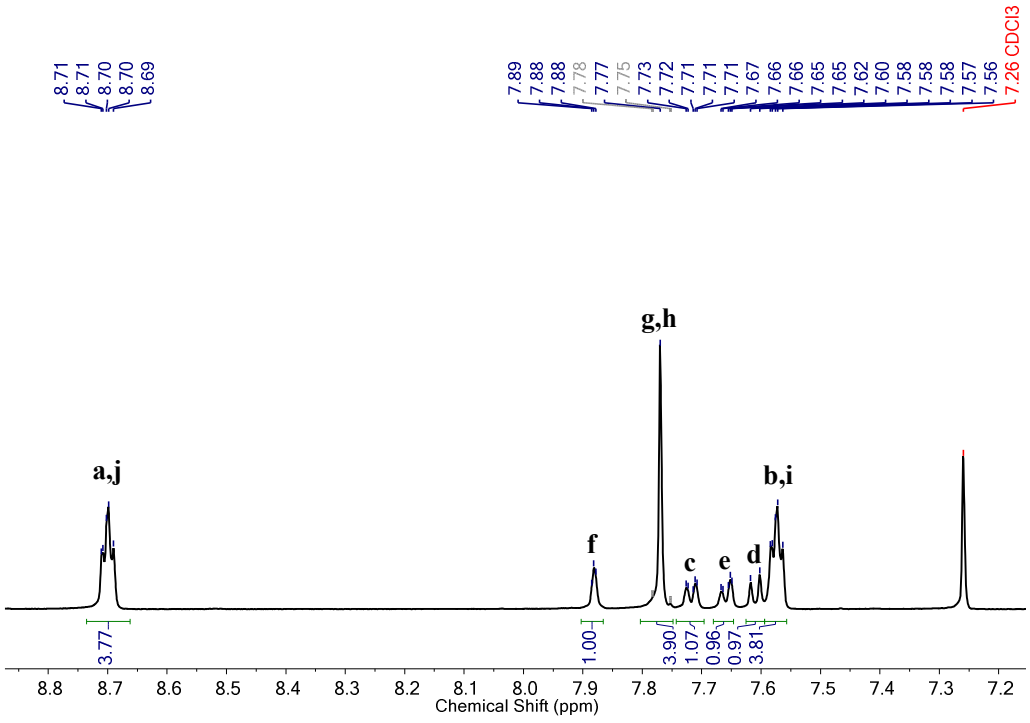

Figure S2. ^{1}H NMR (500 MHz, $CDCl_3$, 300 K) spectrum of $\mathbf{L^A}$ (aromatic region).

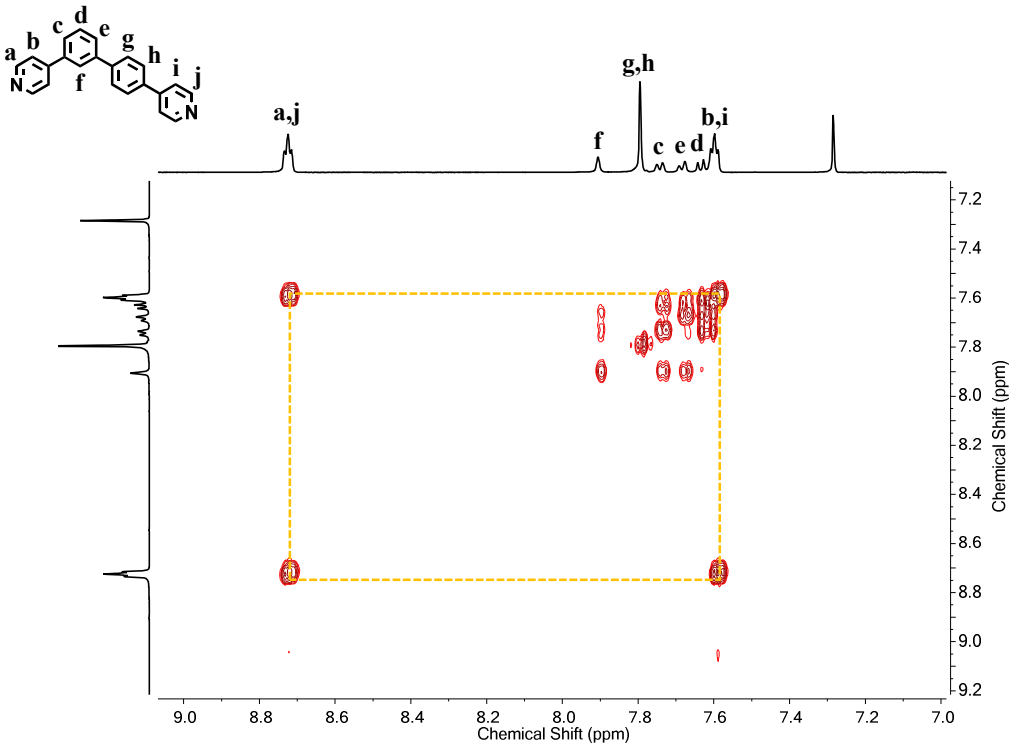

Figure S3. 2D COSY NMR (500 MHz, $CDCl_3$, 300 K) spectrum of $\mathbf{L^A}$ (aromatic region).

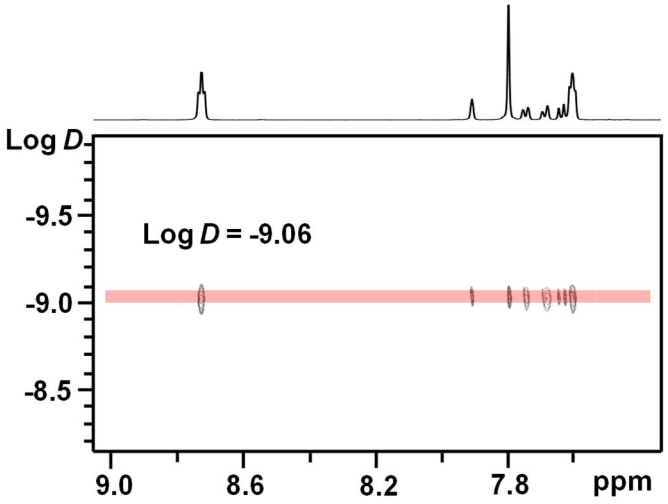

Figure S4. 2D DOSY NMR (500 MHz, $CDCl_3$, 300 K) spectrum of $\mathbf{L^A}$.

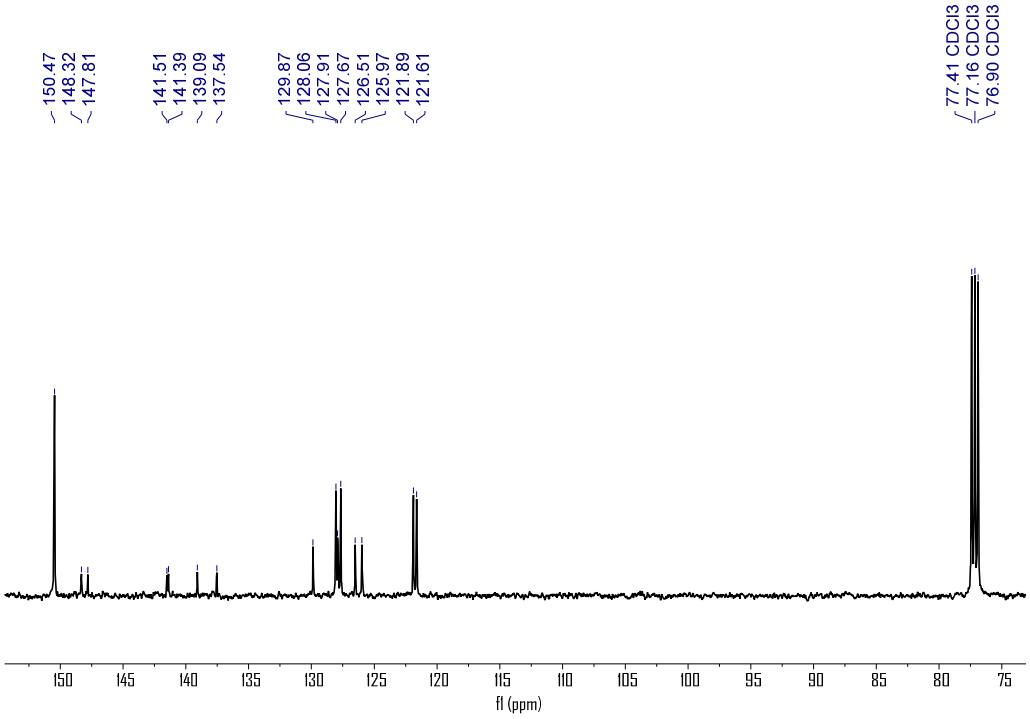

Figure S5. ^{13}C NMR (125 MHz, $CDCl_3$, 300 K) spectrum of $\mathbf{L^A}$.

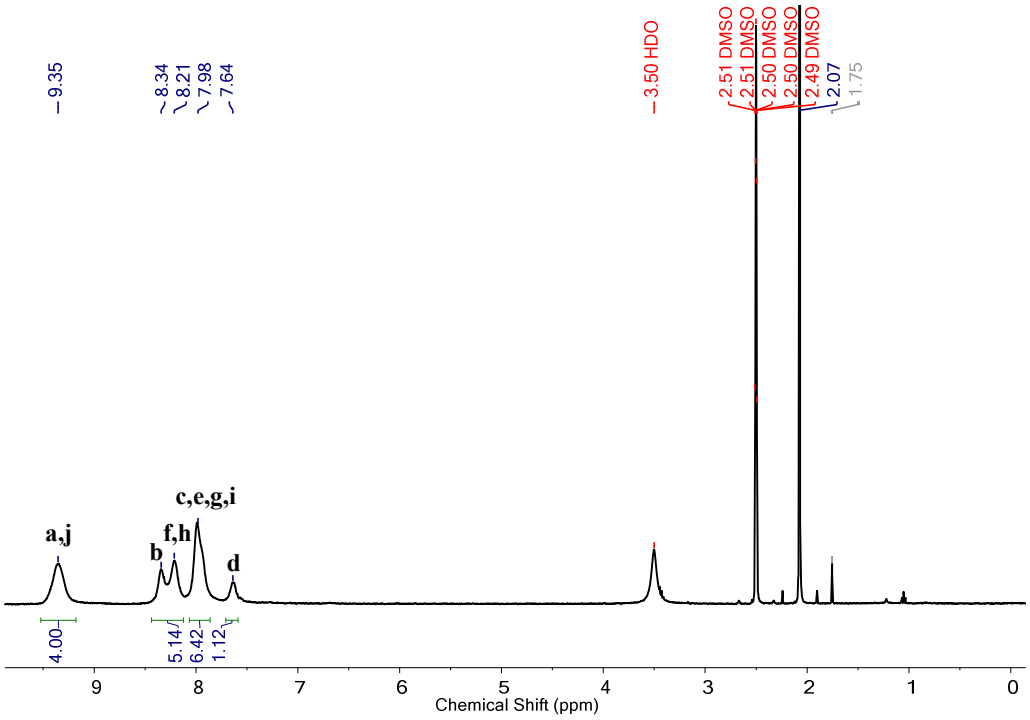

Figure S6. ^{1}H NMR (500 MHz, DMSO-d_6, 300 K) spectrum of $\mathbf{Pd_{12}L^A_{24}}$.

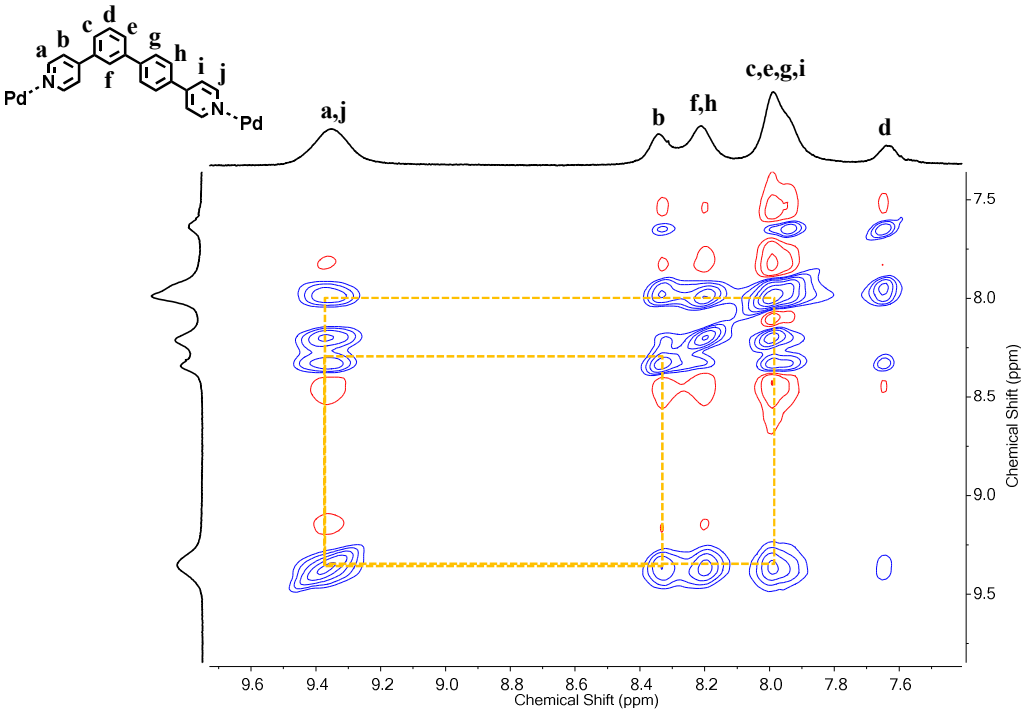

Figure S7. 2D NOESY NMR (600 MHz, DMSO-d_6, 300 K) spectrum of $\mathbf{Pd_{12}L^{A}_{24}}$ (aromatic region).

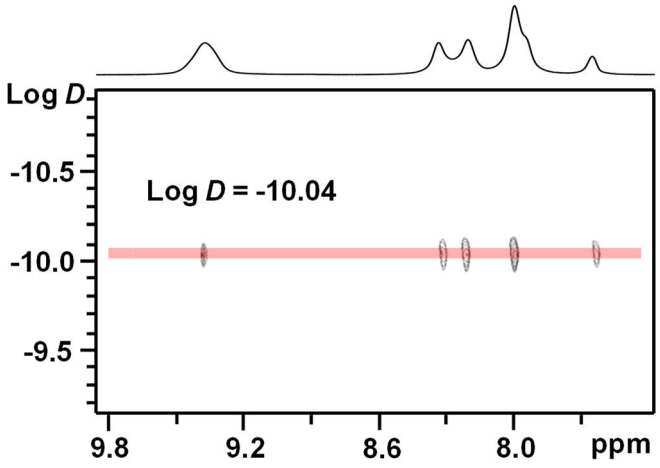

Figure S8. 2D DOSY NMR (500 MHz, DMSO-d_6, 300 K) spectrum of $\mathbf{Pd_{12}L^{A}_{24}}$.

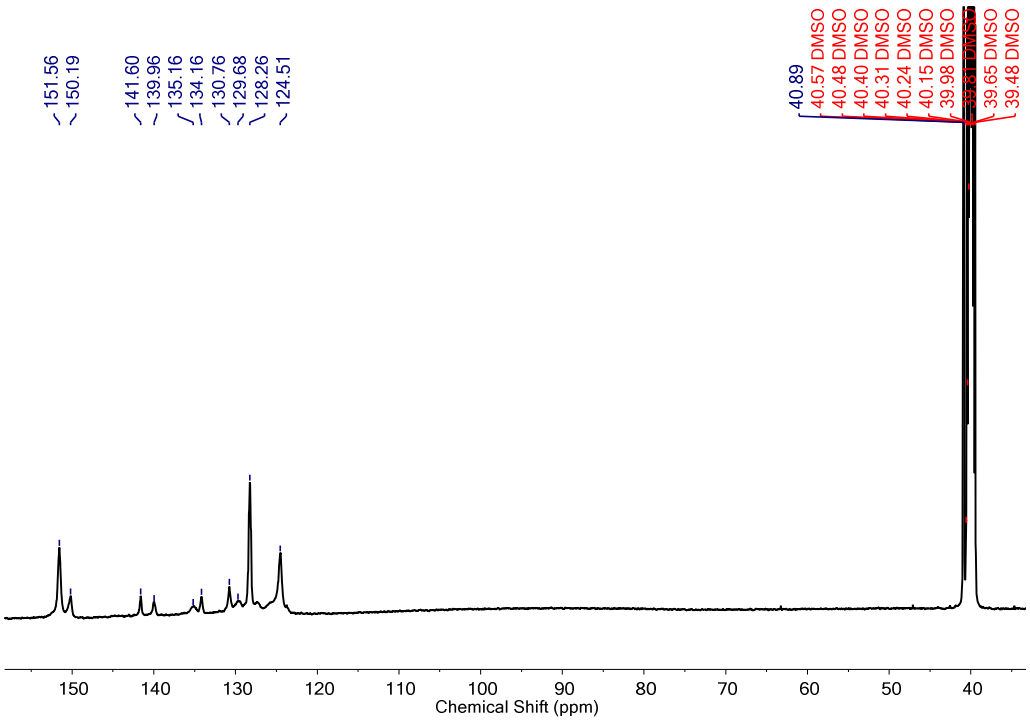

Figure S9. ^{13}C NMR (125 MHz, DMSO-d_6, 300 K) spectrum of $\mathbf{Pd_{12}L^{A}_{24}}$.

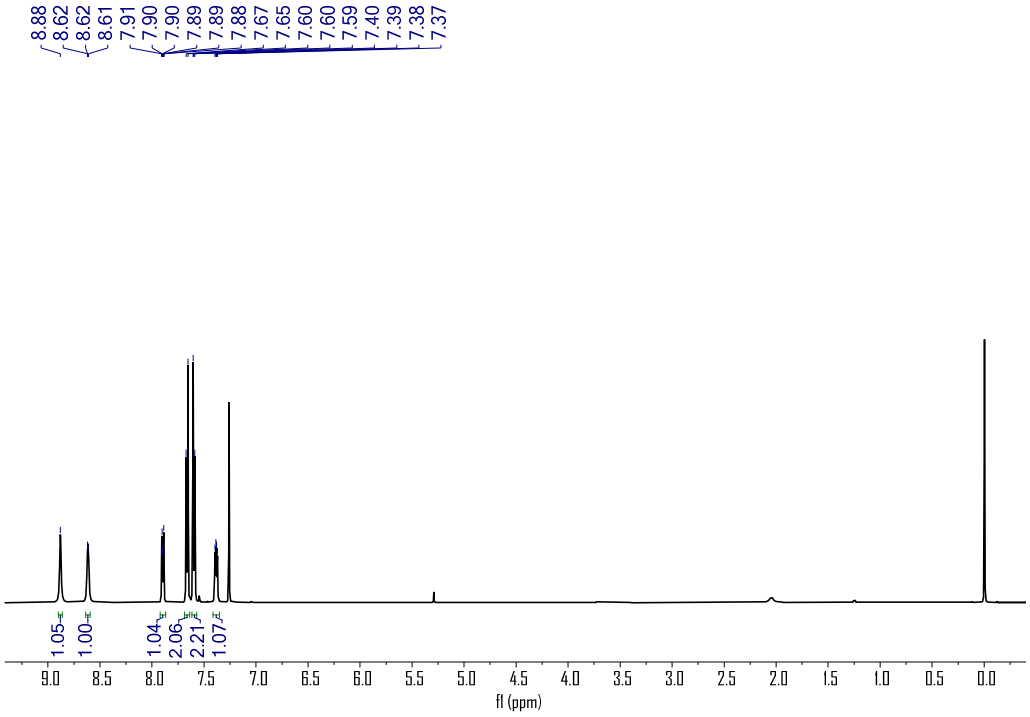

Figure S10. ^{1}H NMR (500 MHz, $CDCl_3$, 300 K) spectrum of $\mathbf{L^{B}}$.

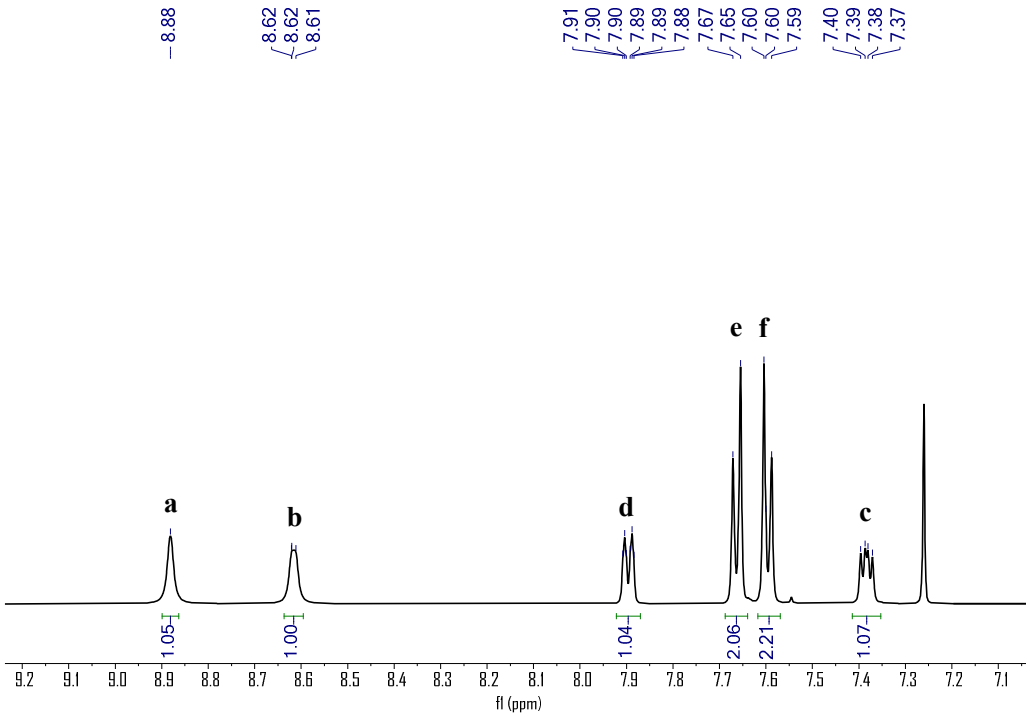

Figure S11. ^{1}H NMR (500 MHz, $CDCl_3$, 300 K) spectrum of $\mathbf{L^B}$ (aromatic region).

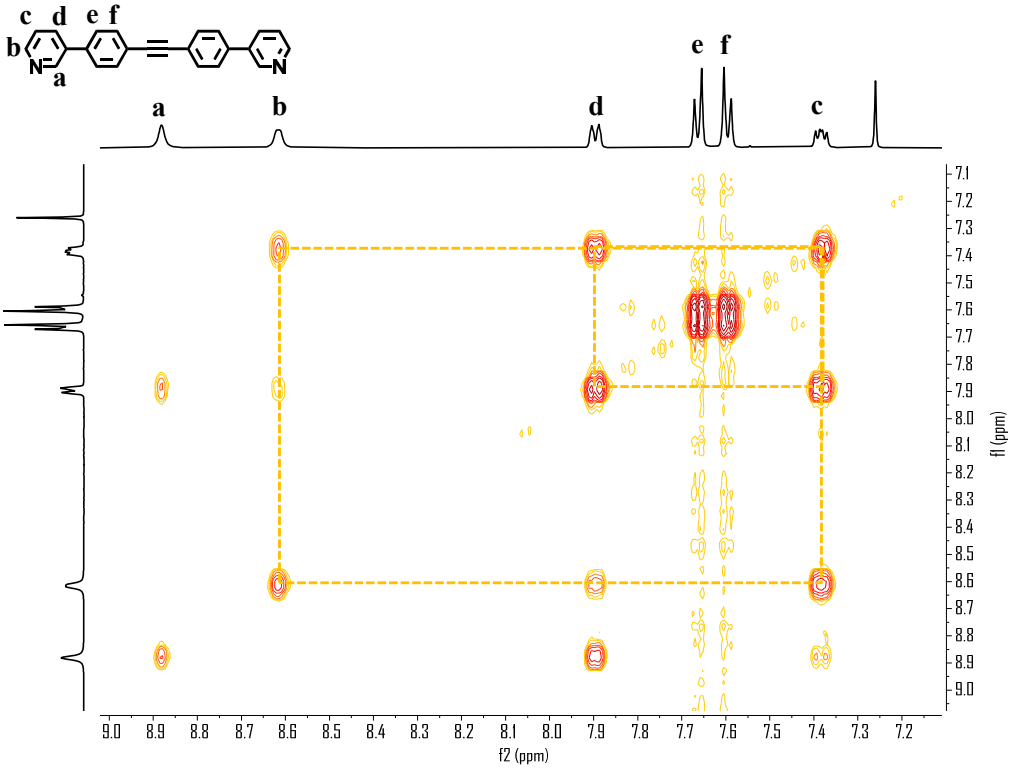

Figure S12. 2D COSY NMR (500 MHz, $CDCl_3$, 300 K) spectrum of $\mathbf{L^B}$ (aromatic region).

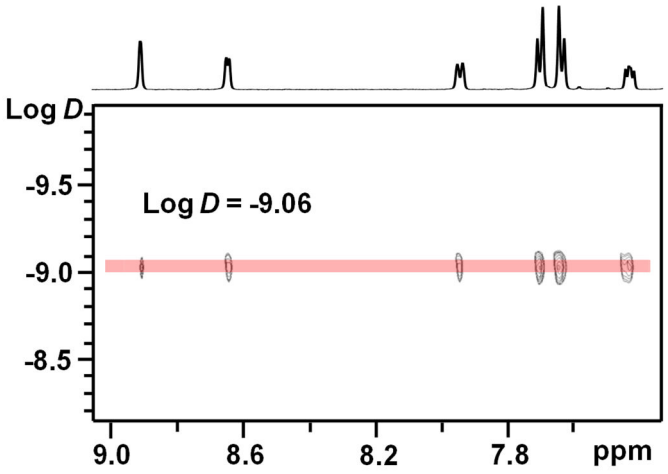

Figure S13. 2D DOSY NMR (500 MHz, $CDCl_3$, 300 K) spectrum of $\mathbf{L^B}$.

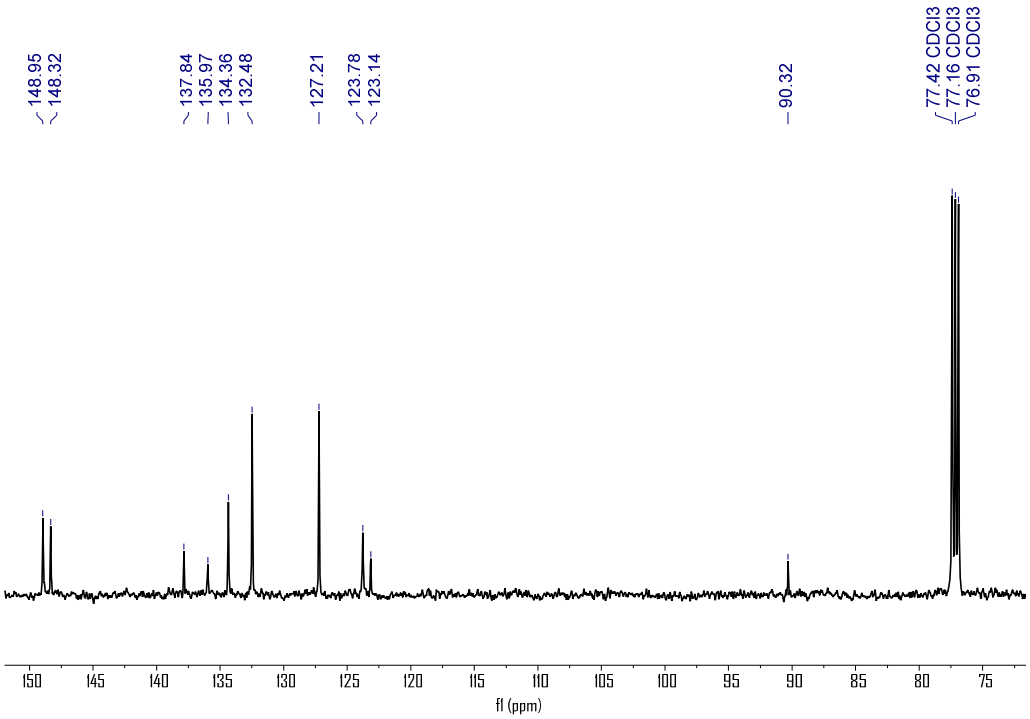

Figure S14. ^{13}C NMR (125 MHz, $CDCl_3$, 300 K) spectrum of $\mathbf{L^B}$.

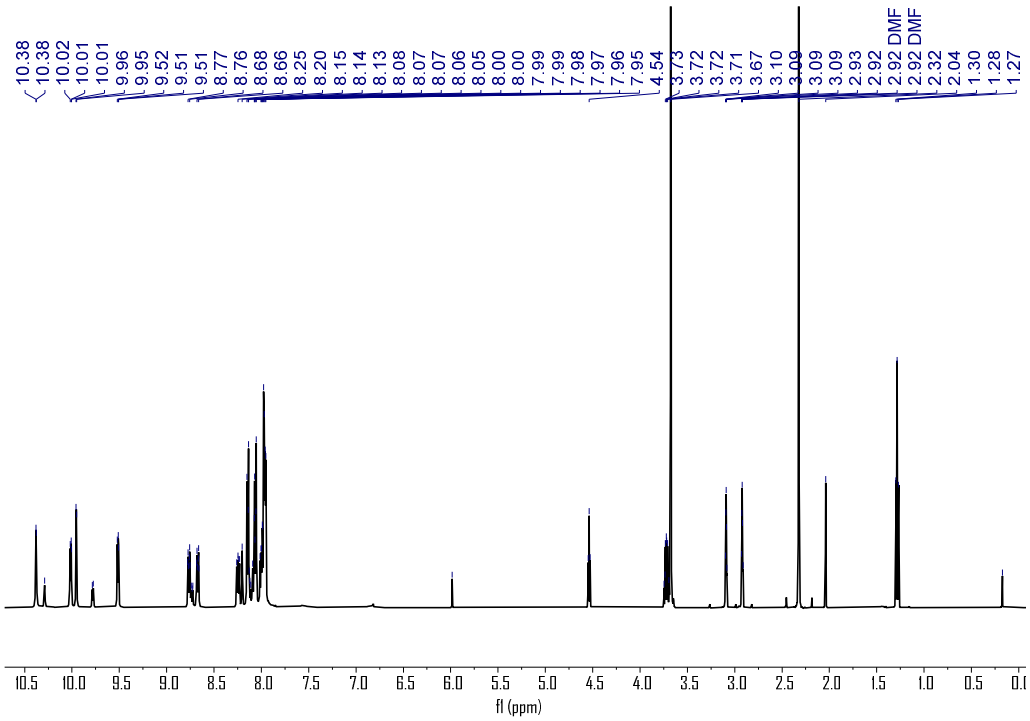

Figure S15. ^{1}H NMR (500 MHz, DMF-d_7, 300 K) spectrum of complexes of $\mathbf{Pd_4L^B_8}$ and $\mathbf{Pd_3L^B_6}$.

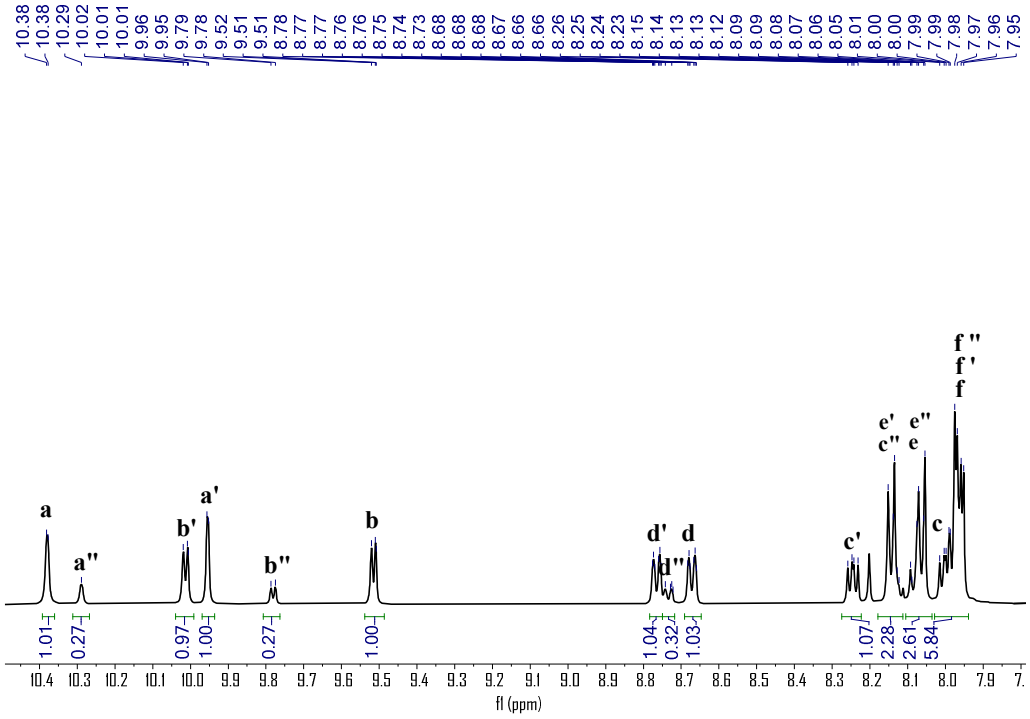

Figure S16. ^{1}H NMR (500 MHz, DMF-d_7, 300 K) spectrum of complexes of $\mathbf{Pd_4L^B_8}$ and $\mathbf{Pd_3L^B_6}$ (aromatic region).

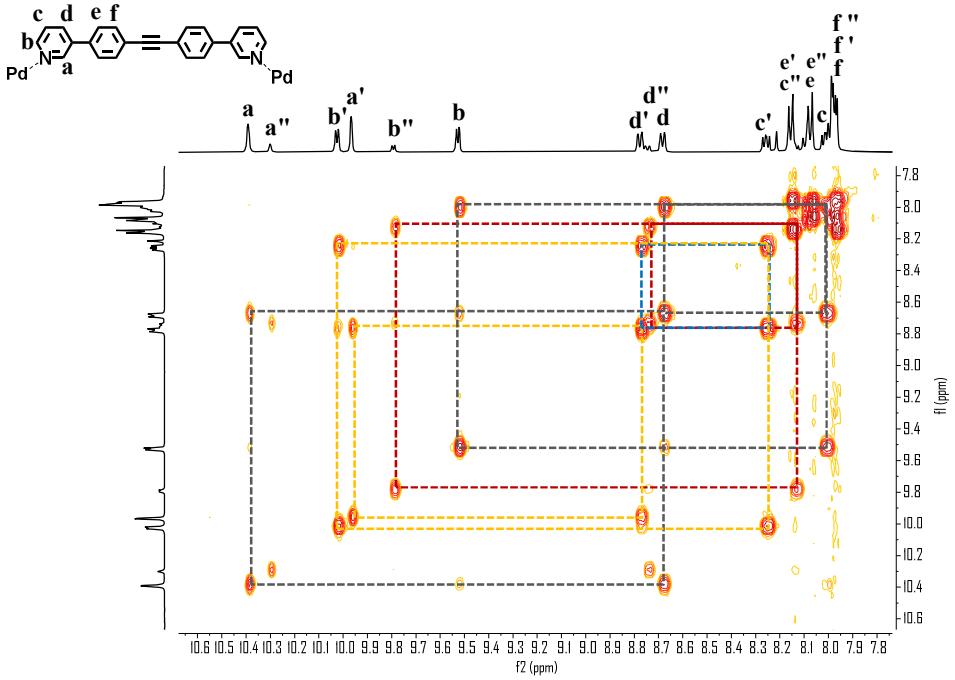

Figure S17. 2D COSY NMR (500 MHz, DMF-d_7, 300 K) spectrum of complexes of $\mathbf{Pd_4L^B_8}$ and $\mathbf{Pd_3L^B_6}$ (aromatic region; a-f and a'-f ' belong to $\mathbf{Pd_4L^B_8}$; a''-f '' belong to $\mathbf{Pd_3L^B_6}$).

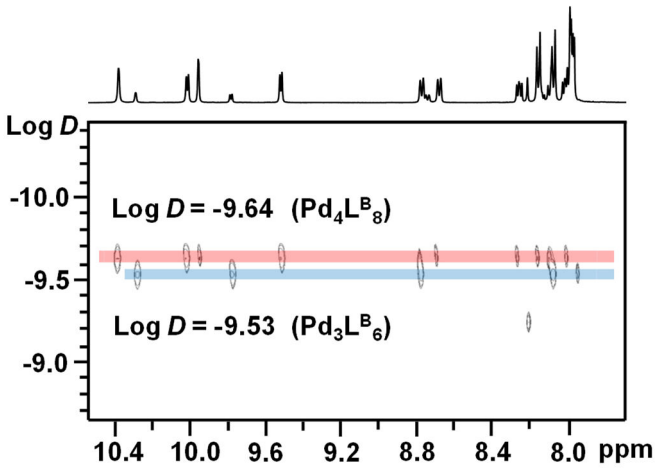

Figure S18. 2D DOSY NMR (500 MHz, DMF-d_7, 300 K) spectrum of complexes of $\mathbf{Pd_4L^B_8}$ and $\mathbf{Pd_3L^B_6}$.

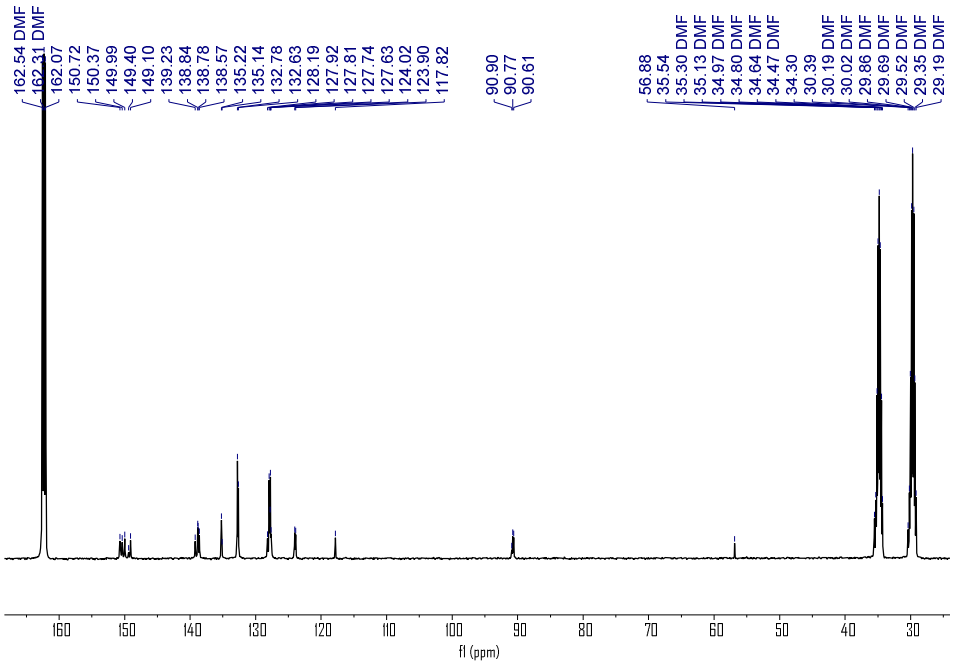

Figure S19. ^{13}C NMR (125 MHz, DMF-d_7, 300 K) spectrum of complexes of $\mathbf{Pd_4L^B_8}$ and $\mathbf{Pd_3L^B_6}$.

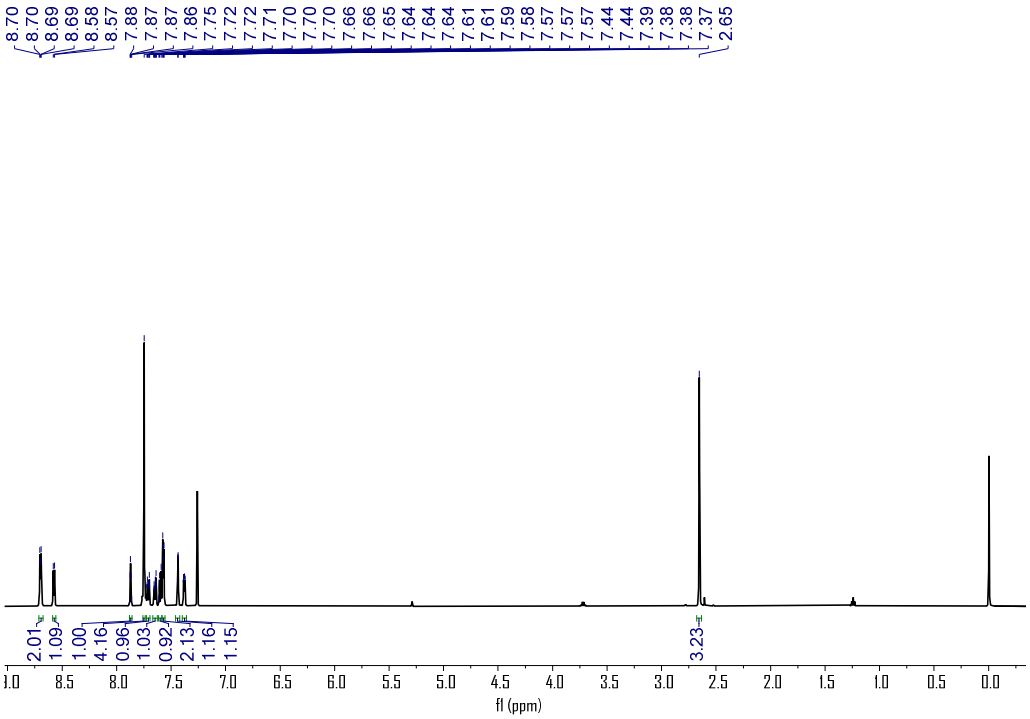

Figure S20. ^{1}H NMR (500 MHz, $CDCl_3$, 300 K) spectrum of $\mathbf{L^C}$.

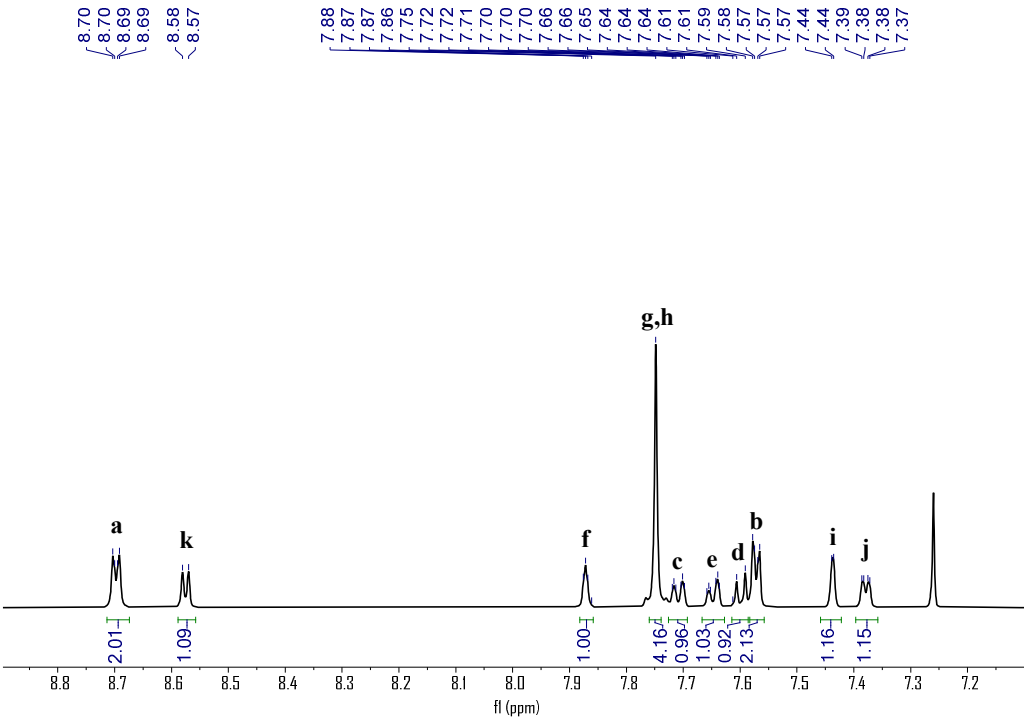

Figure S21. ^{1}H NMR (500 MHz, $CDCl_3$, 300 K) spectrum of $\mathbf{L}^{C}$ (aromatic region).

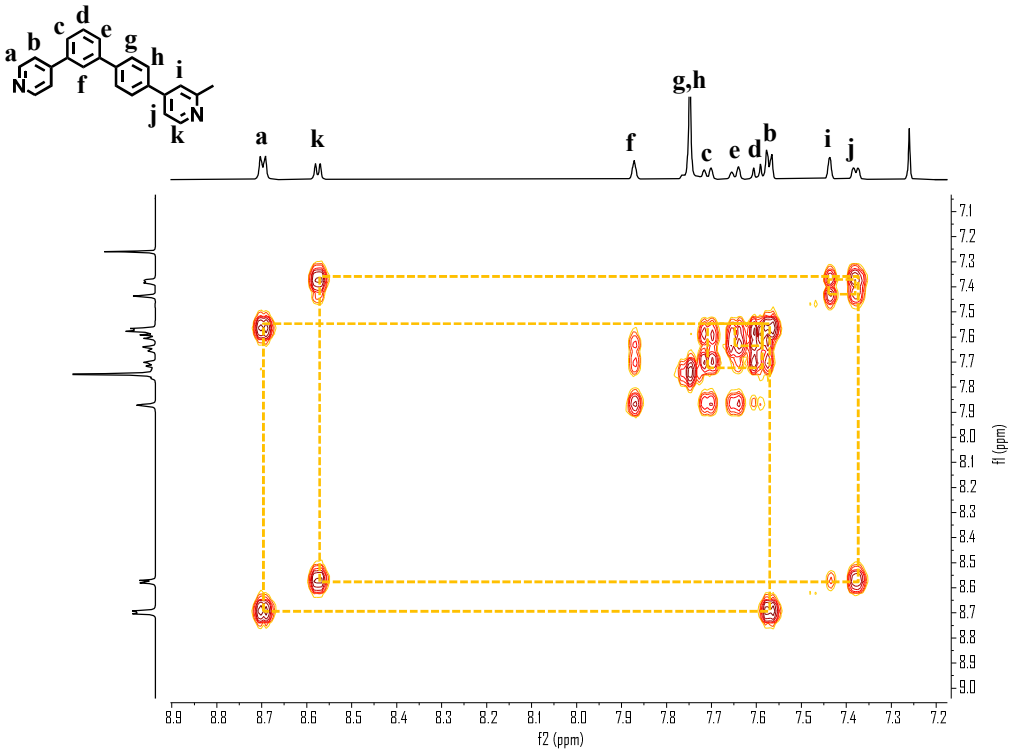

Figure S22. 2D COSY NMR (500 MHz, $CDCl_3$, 300 K) spectrum of $\mathbf{L}^{C}$ (aromatic region).

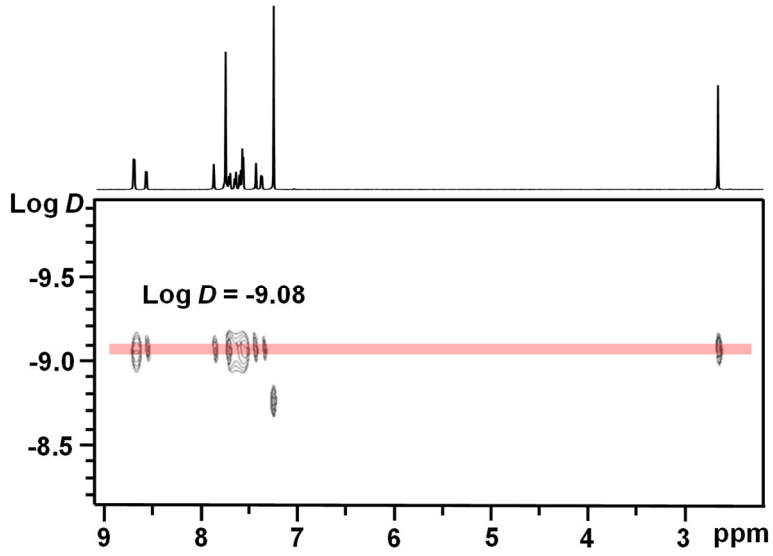

Figure S23. 2D DOSY NMR (500 MHz, $CDCl_3$, 300 K) spectrum of $\mathbf{L}^{C}$.

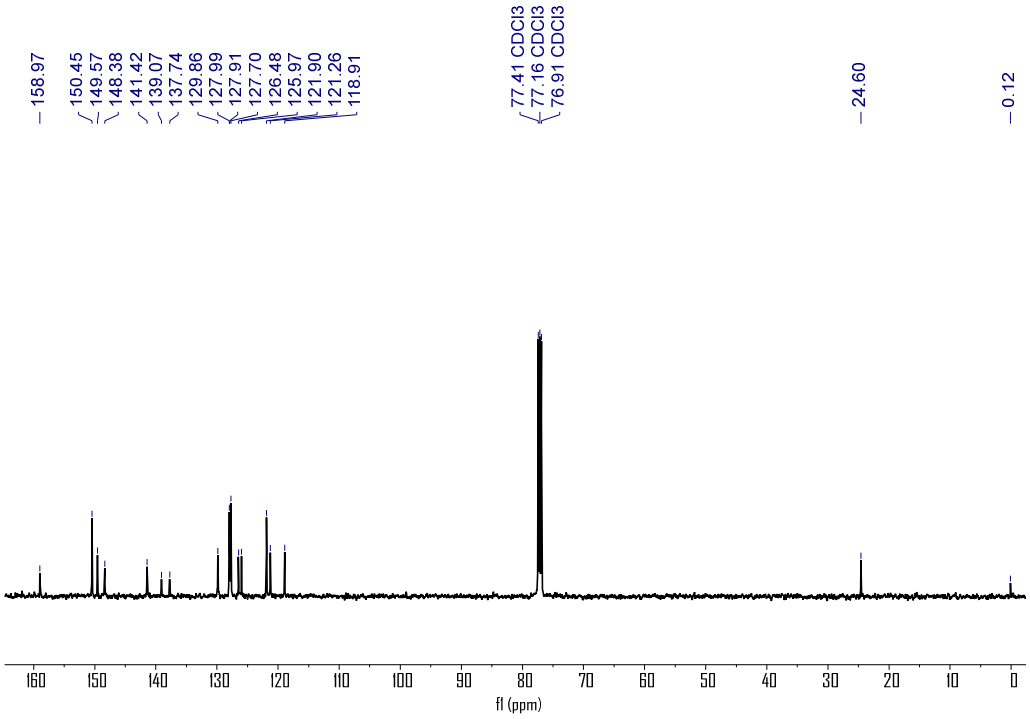

Figure S24. ^{13}C NMR (125 MHz, $CDCl_3$, 300 K) spectrum of $\mathbf{L}^{C}$.

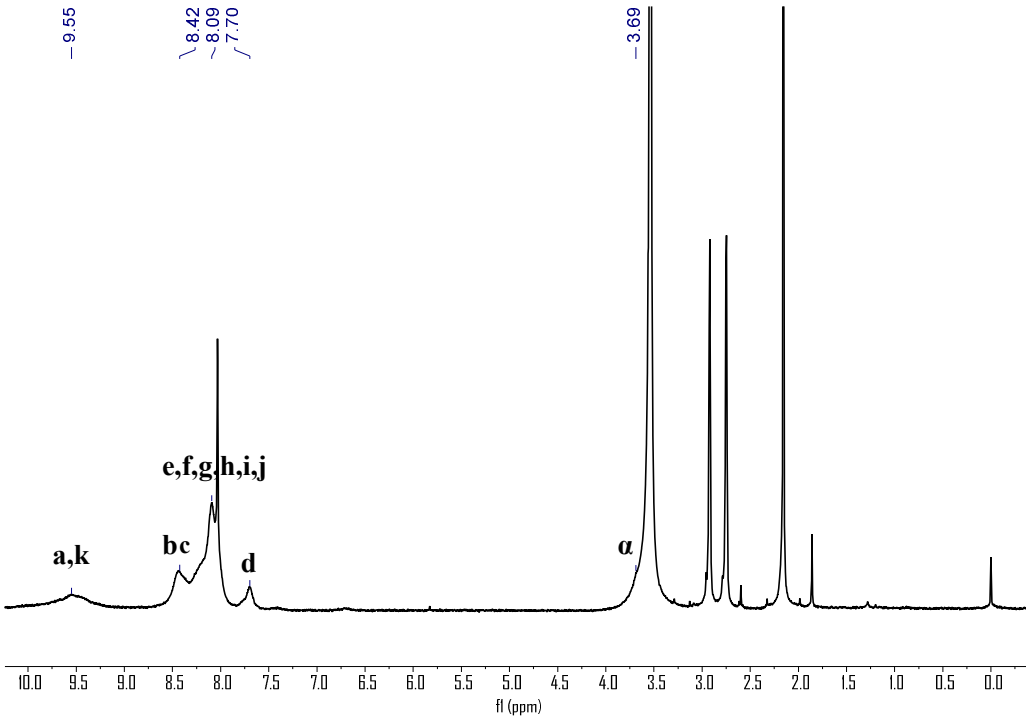

Figure S25. ^{1}H NMR (500 MHz, DMF-d_7, 300 K) spectrum of $\mathbf{Pd_{12}L^{C}_{24}}$.

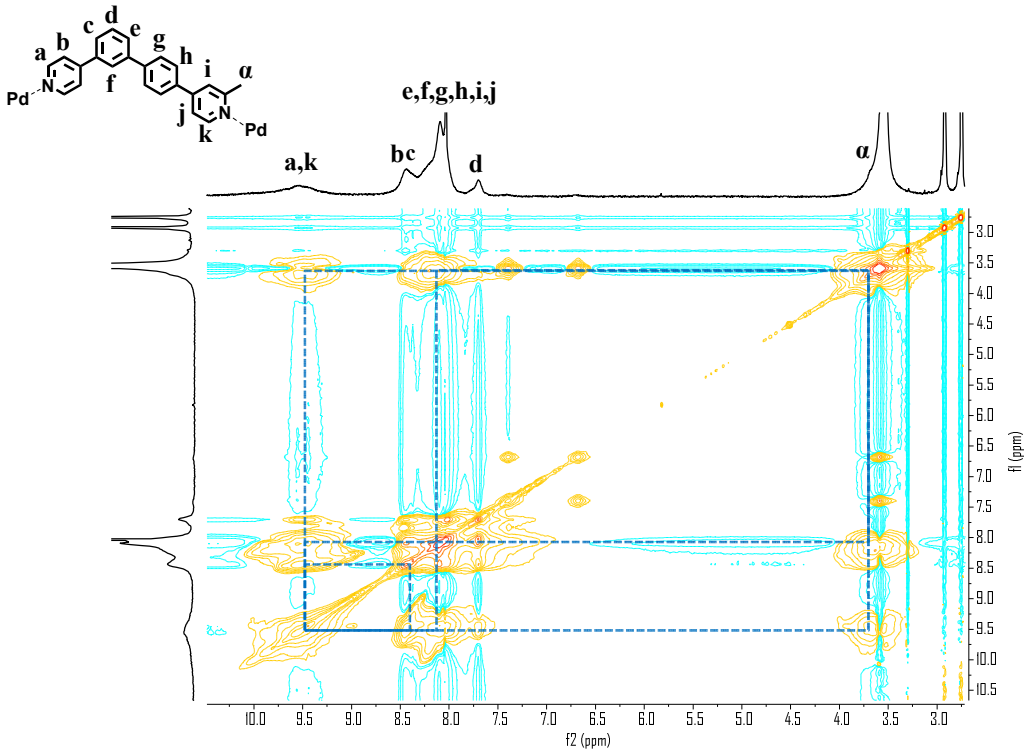

Figure S26. 2D NOESY NMR (600 MHz, DMF-d_7, 300 K) spectrum of $\mathbf{Pd_{12}L^{C}_{24}}$.

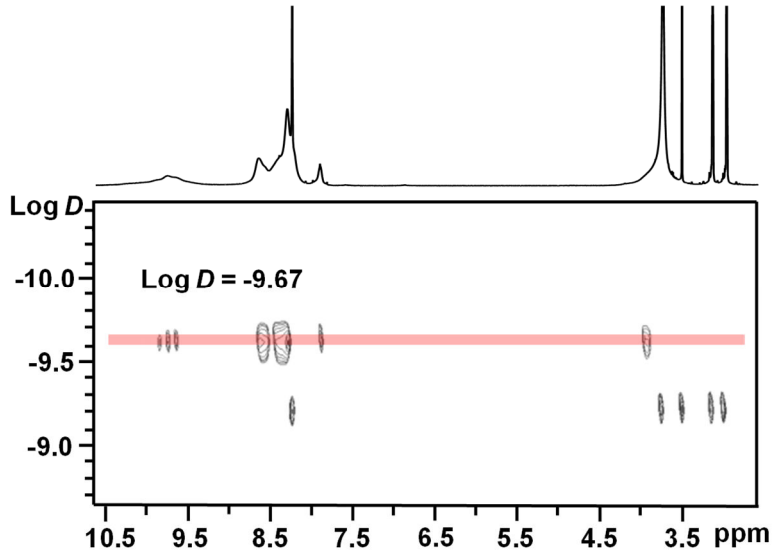

Figure S27. 2D DOSY NMR (500 MHz, DMF-d_7, 300 K) spectrum of $\mathbf{Pd_{12}L^{C}_{24}}$.

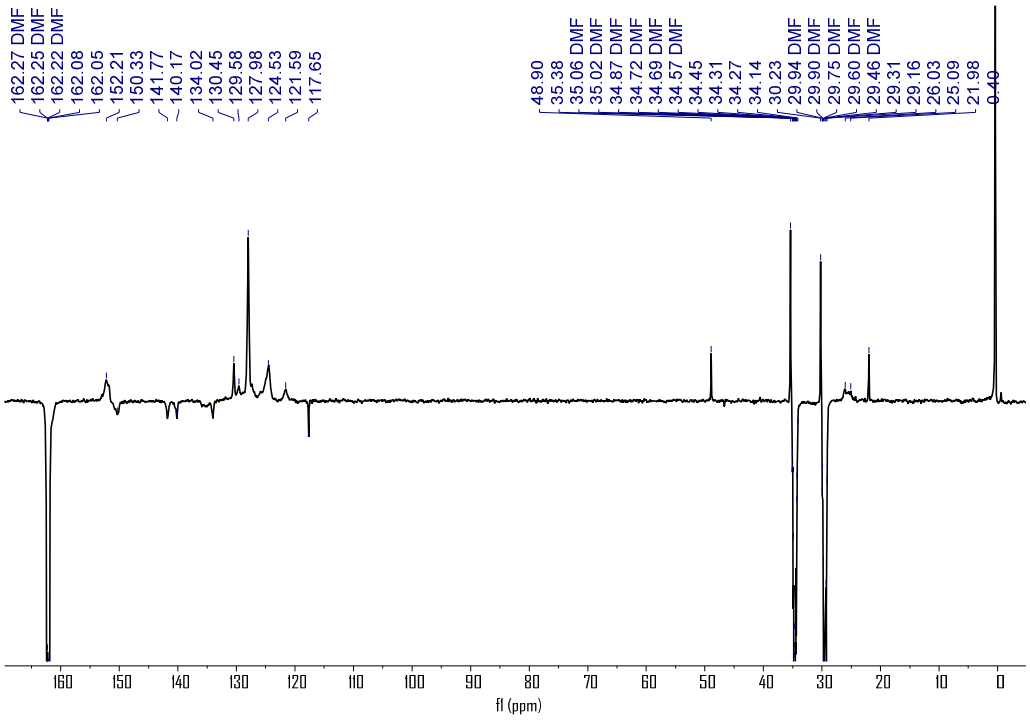

Figure S28. ^{13}C DEPTQ NMR (125 MHz, DMF-d_7, 300 K) spectrum of $\mathbf{Pd_{12}L^{C}_{24}}$.

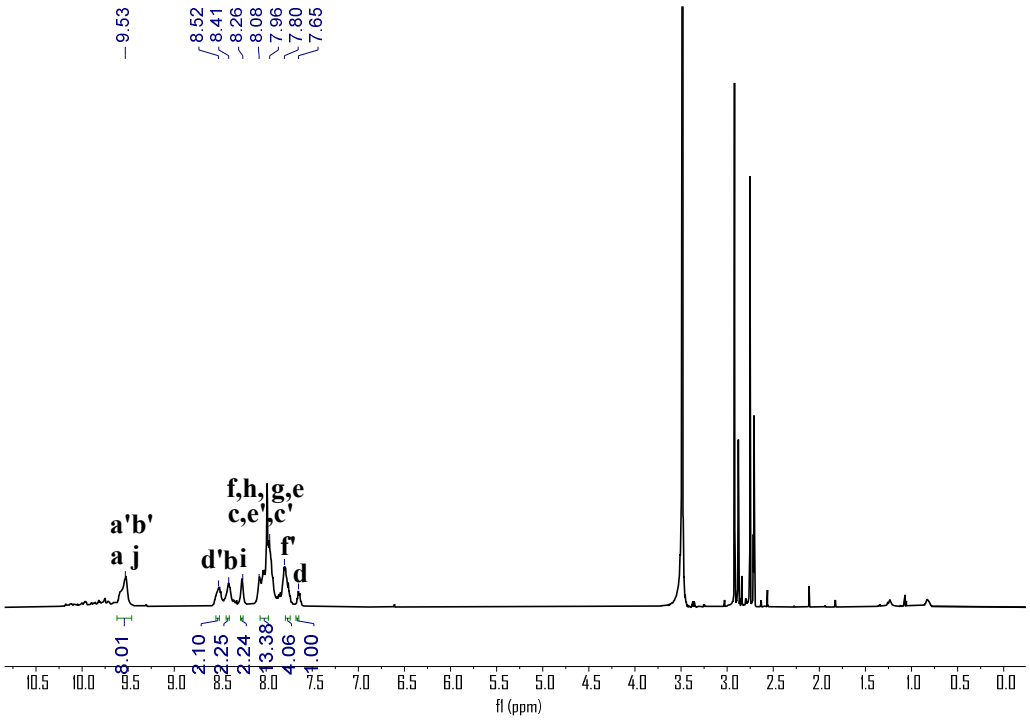

Figure S29. ^{1}H NMR (500 MHz, DMF-d_7, 300 K) spectrum of $\mathbf{Pd_6L^A{}_6L^B{}_6}$.

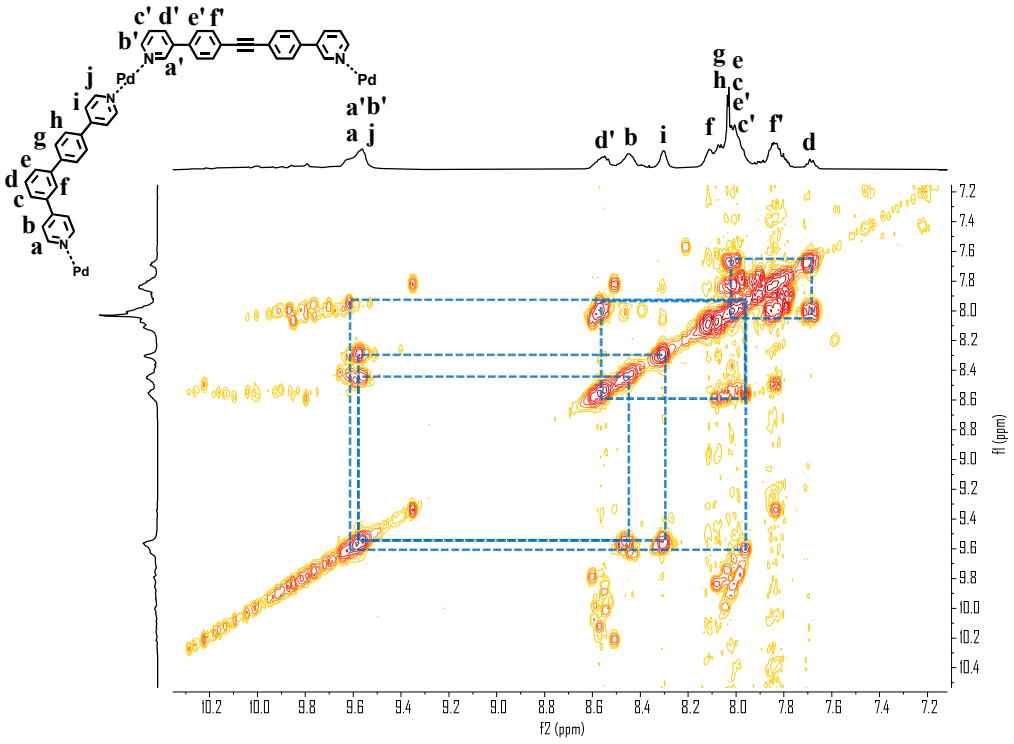

Figure S30. 2D COSY NMR (600 MHz, DMF-d_7, 300 K) spectrum of $\mathbf{Pd_6L^A{}_6L^B{}_6}$.

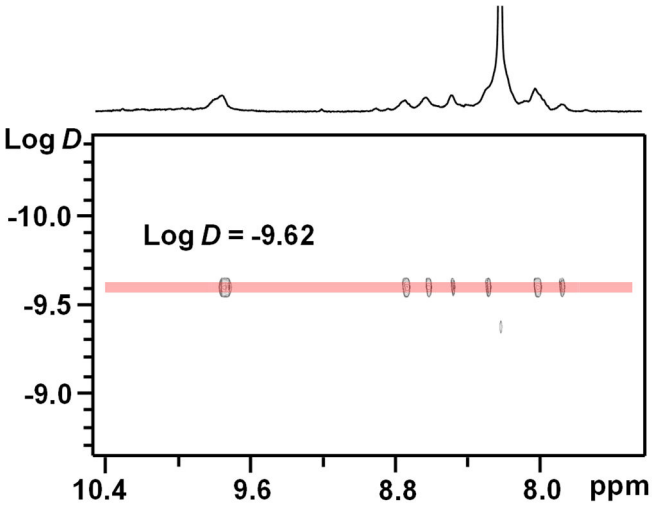

Figure S31. 2D DOSY NMR (500 MHz, DMF-d_7, 300 K) spectrum of $\mathbf{Pd_6L^A{}_6L^B{}_6}$.

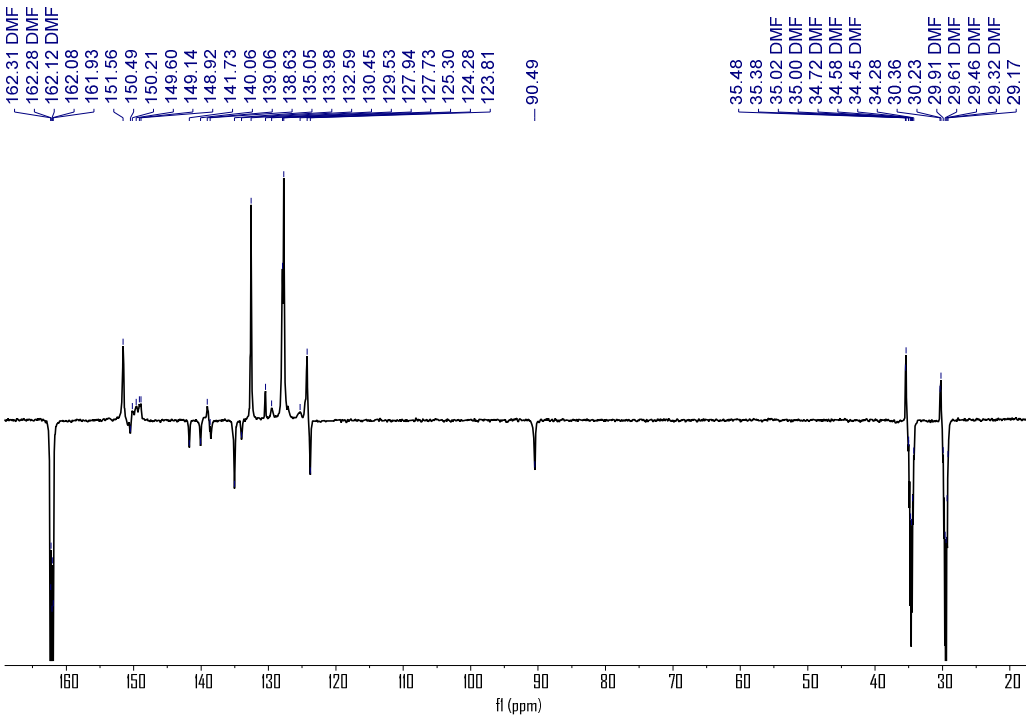

Figure S32. ^{13}C DEPTQ NMR (125 MHz, DMF-d_7, 300 K) spectrum of $\mathbf{Pd_6L^A{}_6L^B{}_6}$.

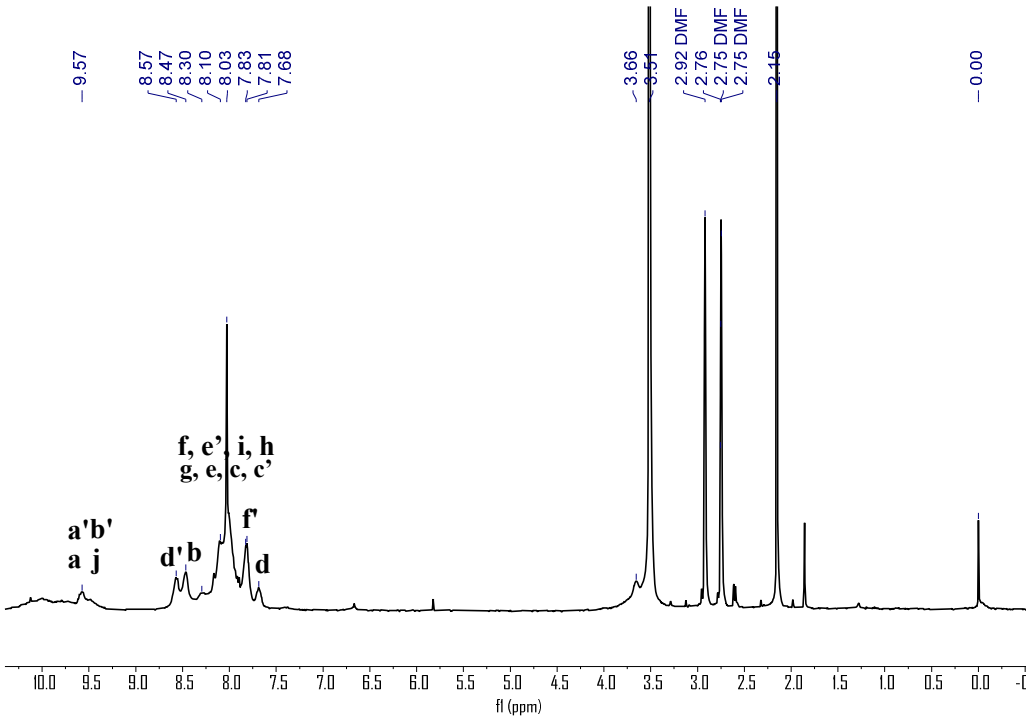

Figure S33. ^{1}H NMR (500 MHz, DMF-d_7, 300 K) spectrum of $\mathbf{Pd_6L^B{}_6L^C{}_6}$.

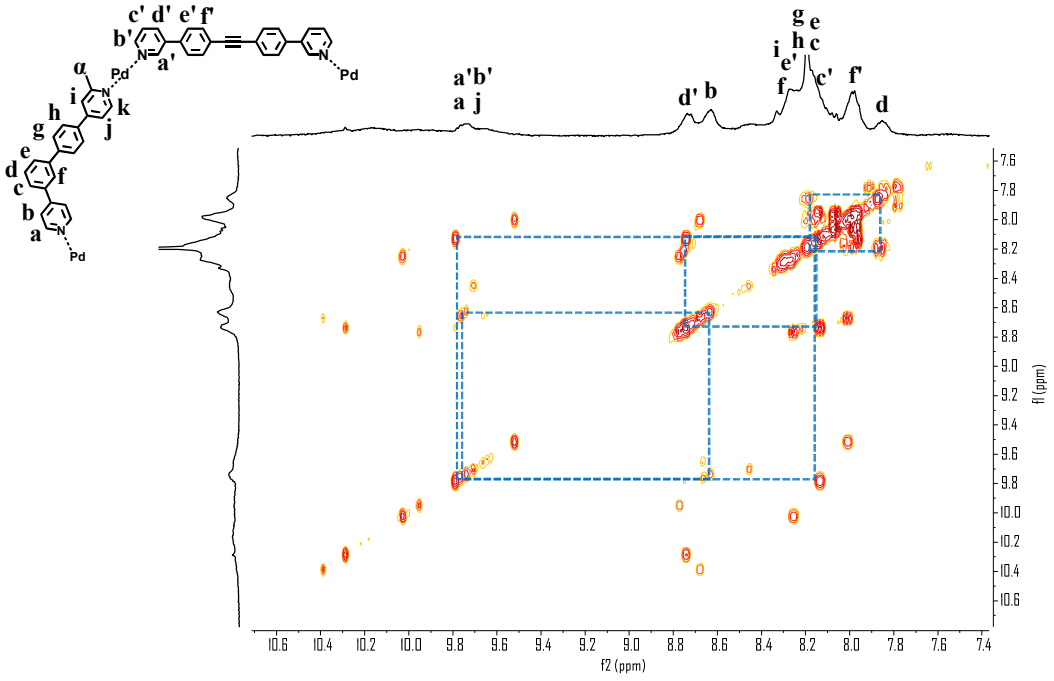

Figure S34. 2D COSY NMR (600 MHz, DMF-d_7, 300 K) spectrum of $\mathbf{Pd_6L^B{}_6L^C{}_6}$.

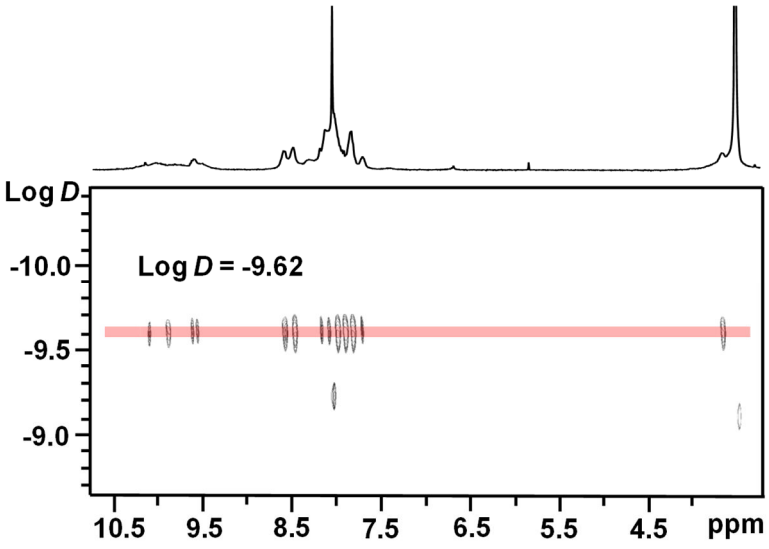

Figure S35. 2D DOSY NMR (500 MHz, DMF-d_7, 300 K) spectrum of $\mathbf{Pd_6L^B{}_6L^C{}_6}$.

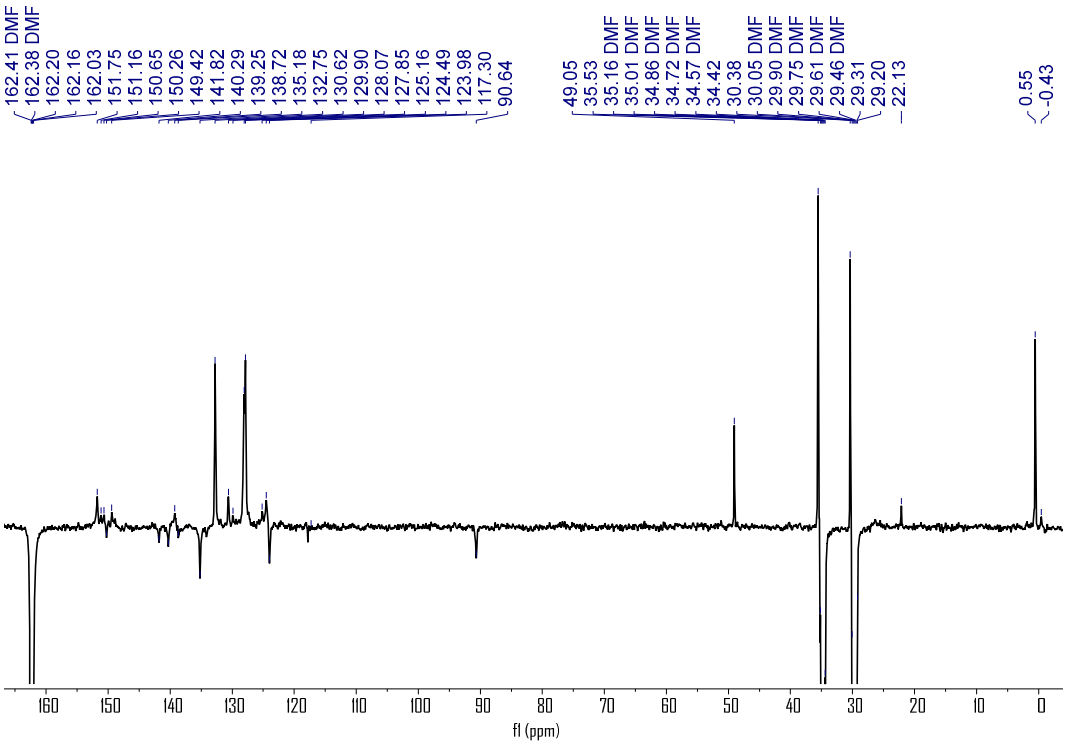

Figure S36. ^{13}C DEPTQ NMR (125 MHz, DMF-d_7, 300 K) spectrum of $\mathbf{Pd_6L^B{}_6L^C{}_6}$.

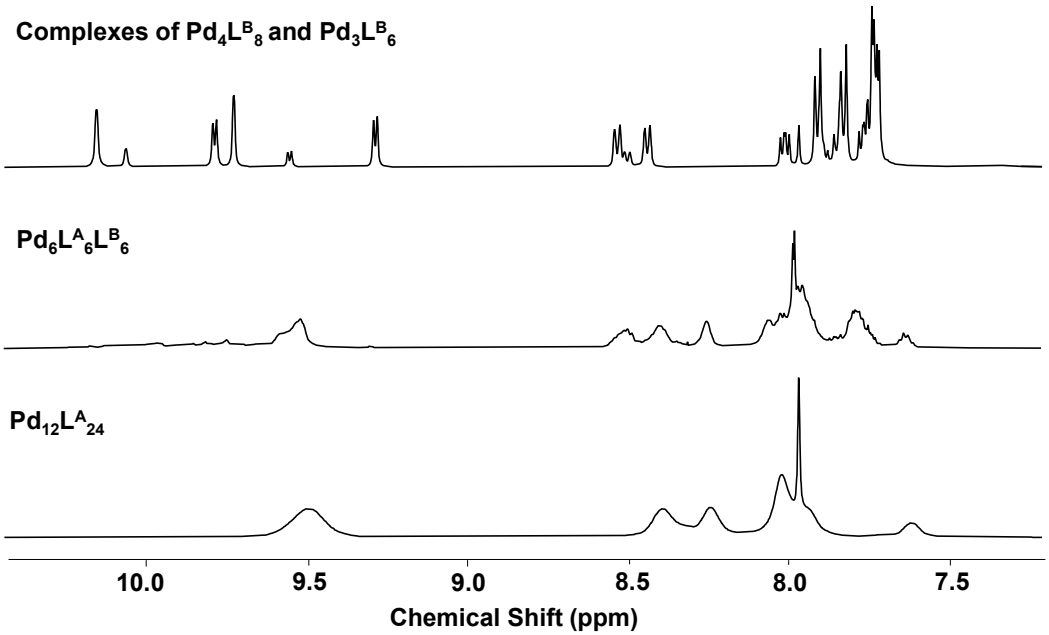

Figure S37. ^{1}H NMR spectra (500 MHz, 300 K) of complexes of $\mathbf{Pd_4L^B_8}$ and $\mathbf{Pd_3L^B_6}$, $\mathbf{Pd_6L^A_6L^B_6}$, and $\mathbf{Pd_{12}L^A_{24}}$ in DMF-d_7.

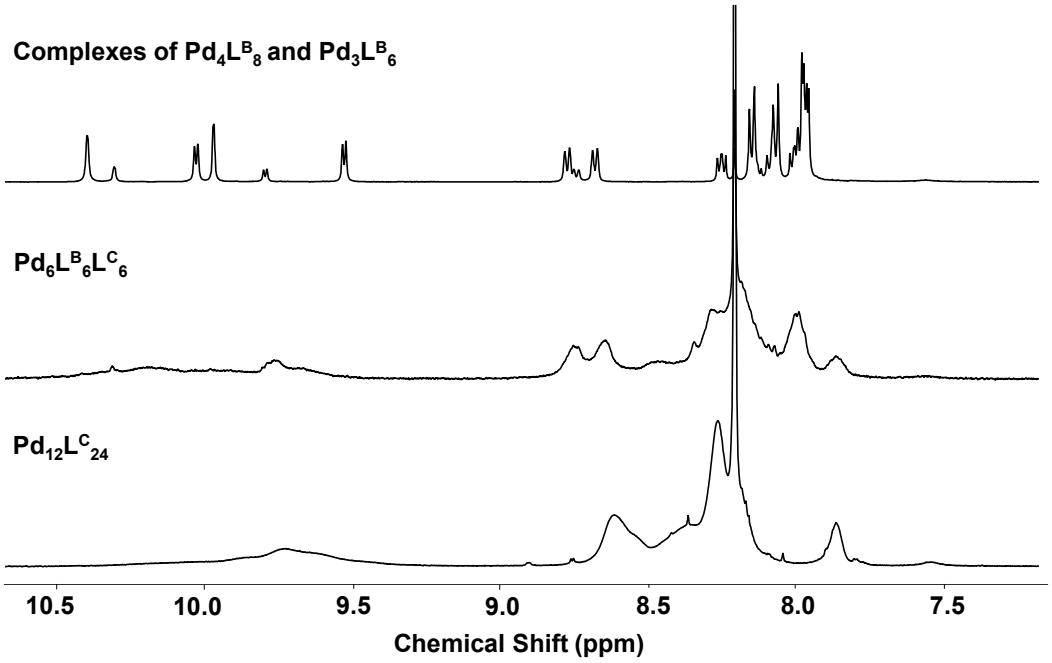

Figure S38. ^{1}H NMR spectra (500 MHz, 300 K) of complexes of $\mathbf{Pd_4L^B_8}$ and $\mathbf{Pd_3L^B_6}$, $\mathbf{Pd_6L^B_6L^C_6}$, and $\mathbf{Pd_{12}L^C_{24}}$ in DMF-d_7.

In the ^{1}H NMR spectrum of $\mathbf{Pd_{12}L^{C}_{24}}$, it can be observed that 9.0-9.75 ppm splits into three groups of peaks. In the variable temperature NMR experiment, as the temperature gradually increased, the degree of splitting of the proton peak at 9.0-9.75 ppm gradually increased (***Figure S39***). When the test temperature reached 353 K, obvious signal splitting of the proton peak at 9.0-9.75 ppm can be observed in the ^{1}H NMR spectrum. We infer that if there are a large number of isomers in $\mathbf{Pd_{12}L^{C}_{24}}$, the proton signal ortho to the nitrogen on pyridine will not be split, but just a broad peak. Therefore, through NMR analysis, it can be preliminarily determined that the ligands in $\mathbf{Pd_{12}L^{C}_{24}}$ are not disordered, but may be arranged in a regular orientation.

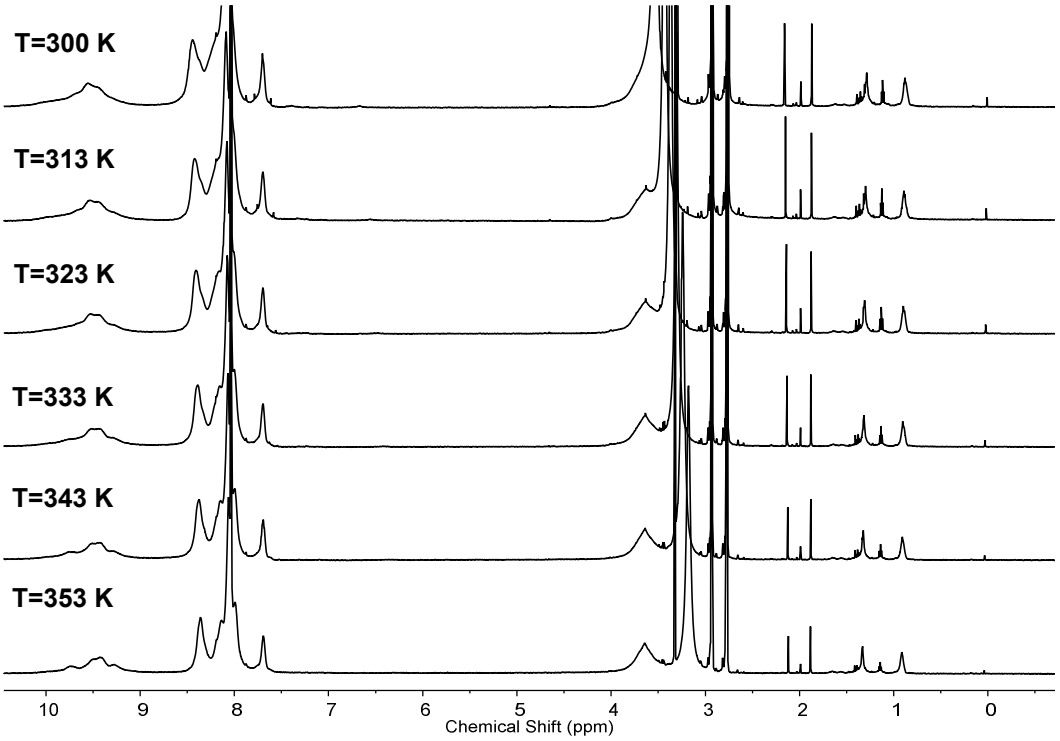

Figure S39. Variable temperature ^{1}H NMR spectra of $\mathbf{Pd_{12}L^{C}_{24}}$ from 300 K to 353 K.

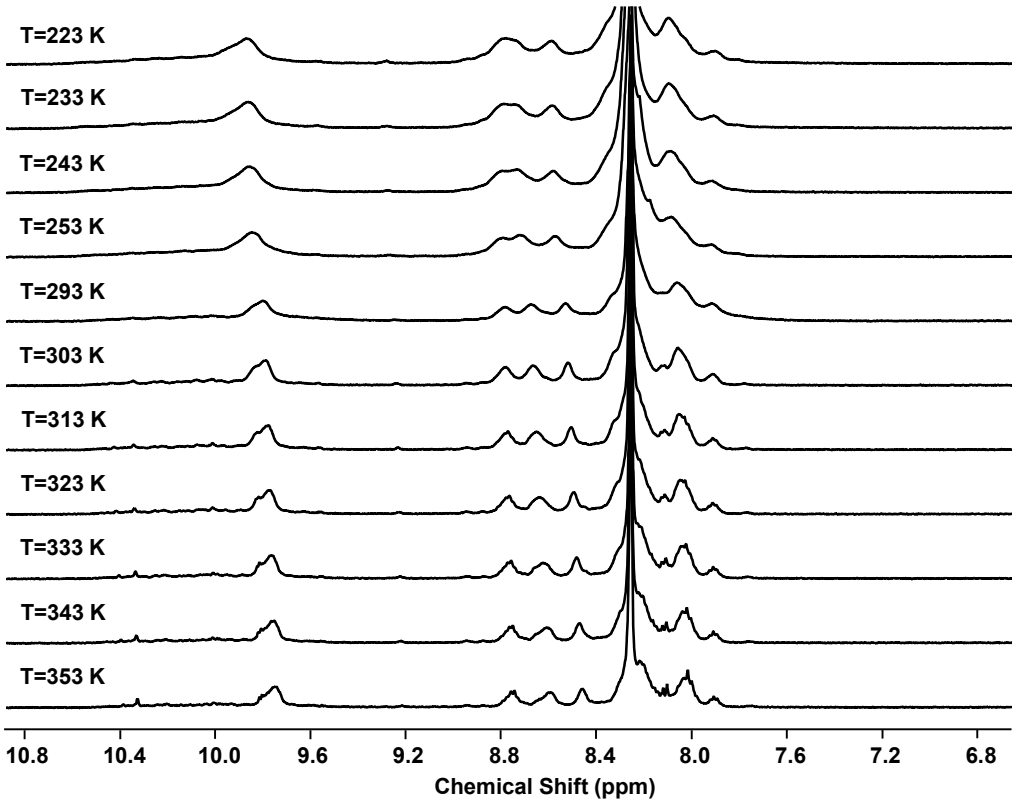

Figure S40. Variable temperature ^{1}H NMR spectra of $\mathbf{Pd_6L^A{}_6L^B{}_6}$ from 223 K to 353 K.

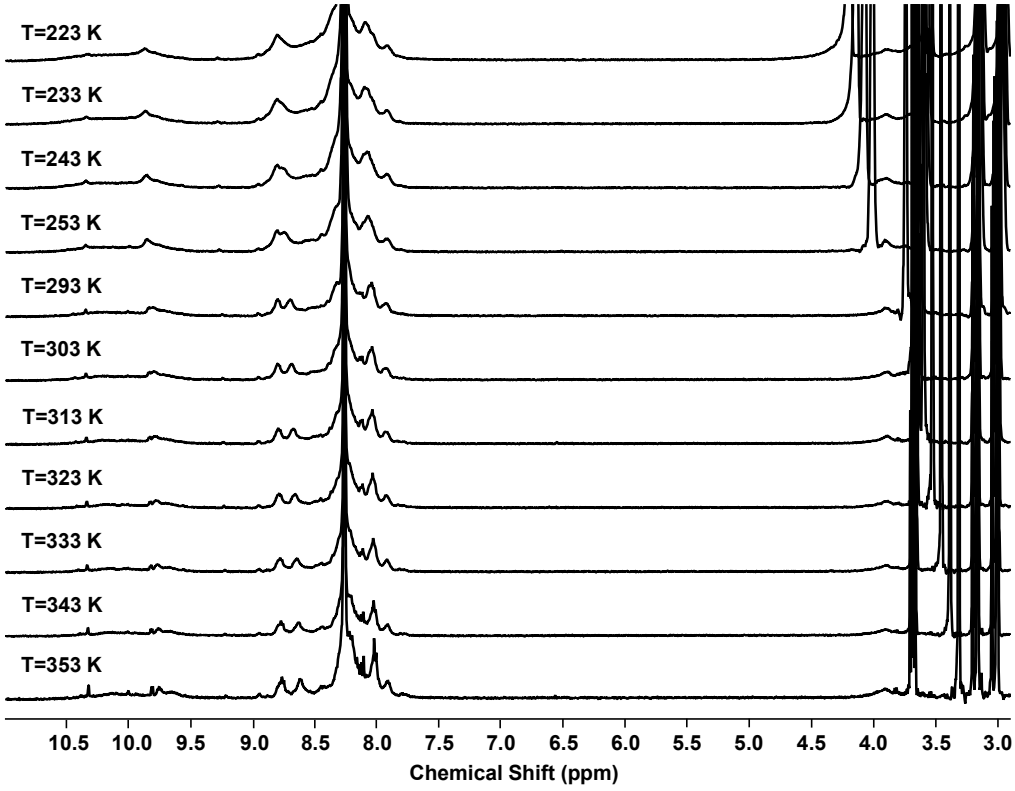

Figure S41. Variable temperature ^{1}H NMR spectra of $\mathbf{Pd_6L^B{}_6L^C{}_6}$ from 223 K to 353 K.

4. ESI-MS Spectra Data of Ligands and Complexes

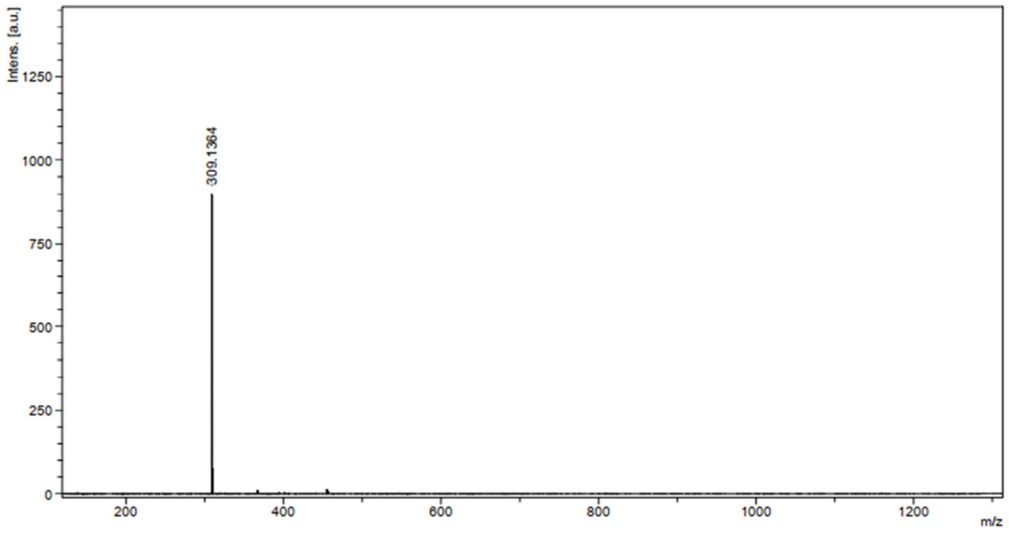

Figure S42. ESI-MS spectrum of $\mathbf{L^A}$.

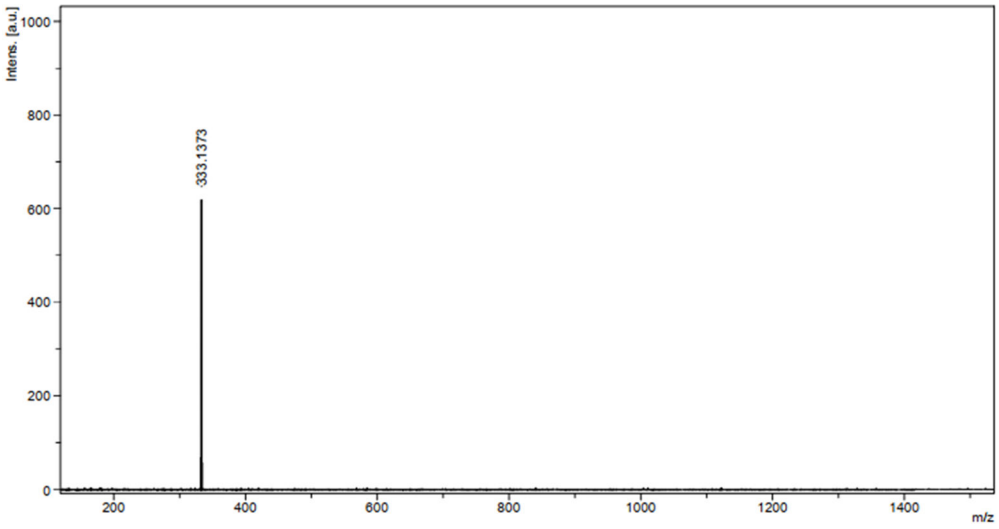

Figure S43. ESI-MS spectrum of $\mathbf{L^B}$.

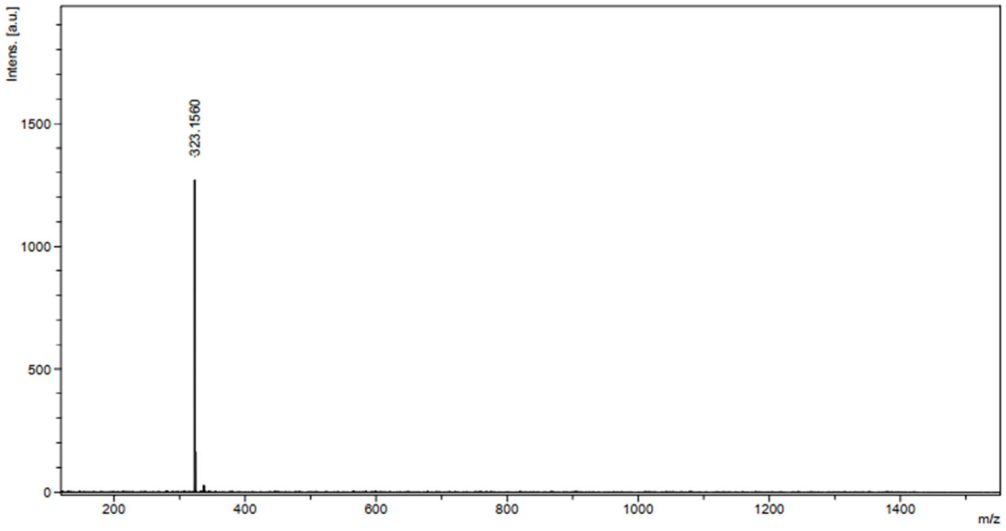

Figure S44. ESI-MS spectrum of $\mathbf{L}^{C}$.

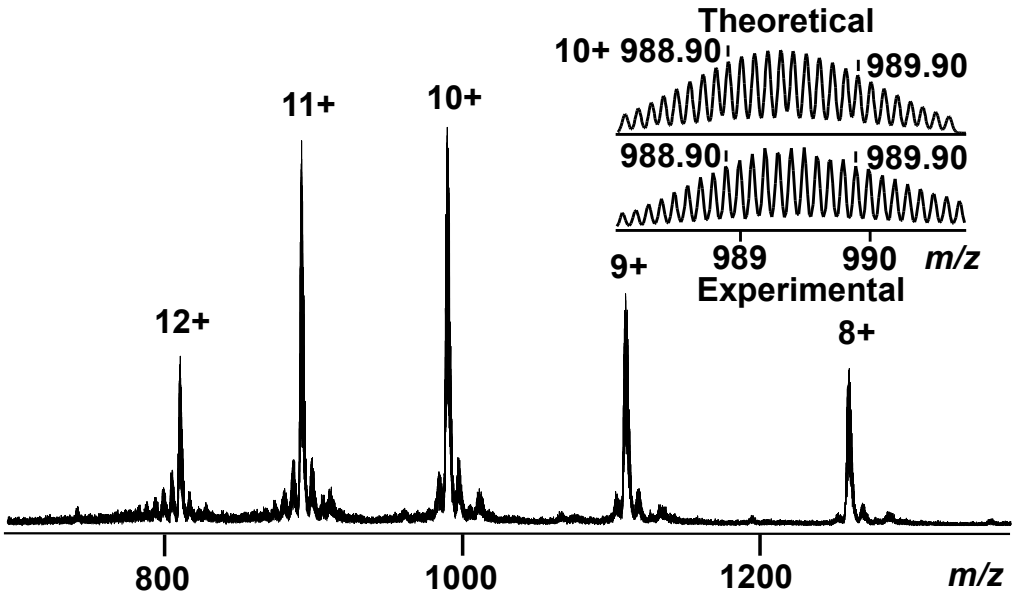

Figure S45. ESI-MS spectrum of cage $\mathbf{Pd_{12}L^{A}_{24}}$ (BF_4^- as counterion).

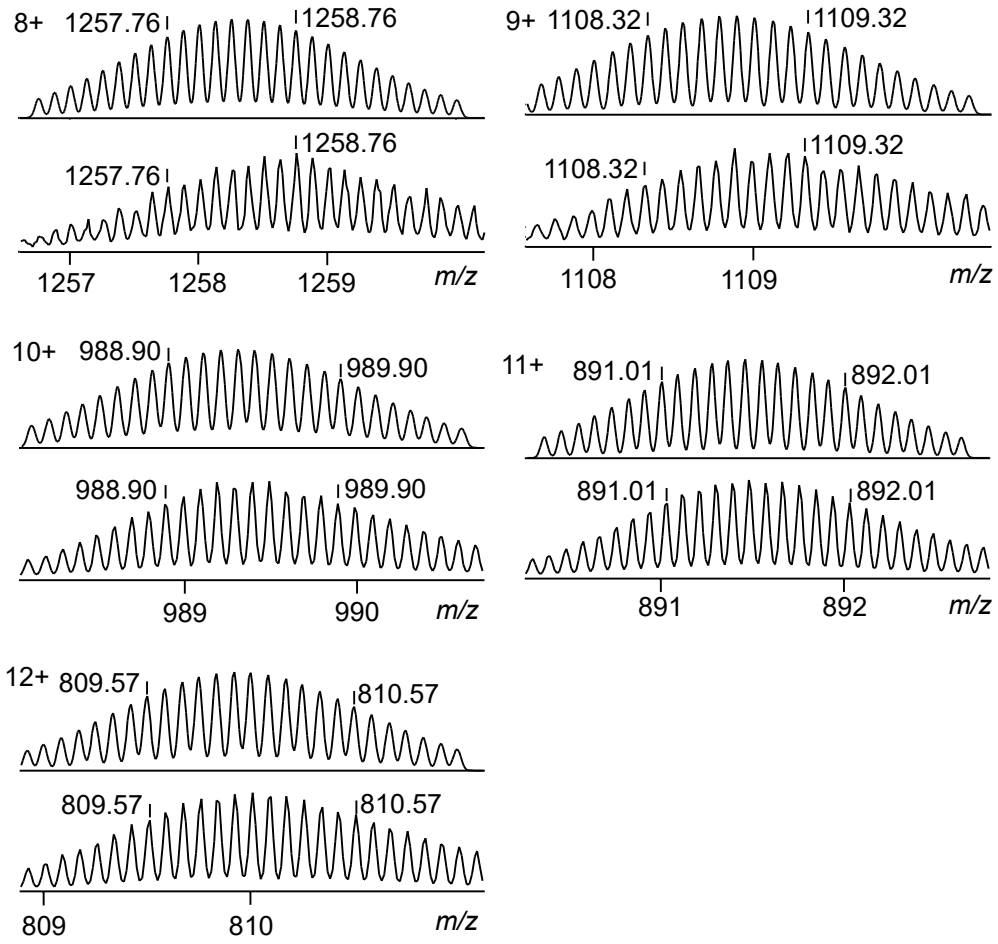

Figure S46. Measured (bottom) and calculated (top) isotope patterns for different charge states observed from $\mathbf{Pd_{12}L^{A}_{24}}$ (BF_4^- as counterion).

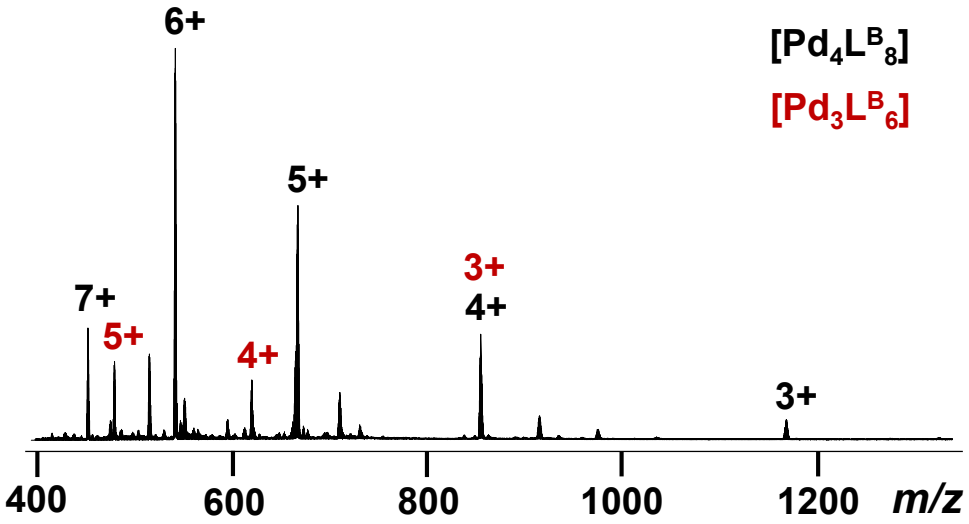

Figure S47. ESI-MS spectrum of complexes of $\mathbf{Pd_4L^{B}_8}$ and $\mathbf{Pd_3L^{B}_6}$ (BF_4^- as counterion).

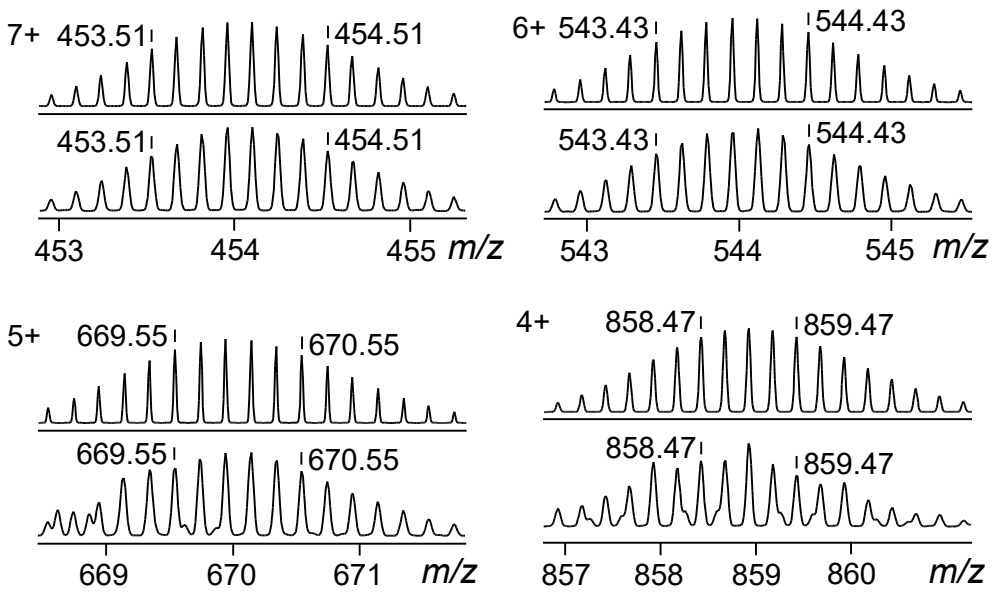

Figure S48. Measured (bottom) and calculated (top) isotope patterns for different charge states observed from $\mathbf{Pd_4L^B_8}$ (BF_4^- as counterion).

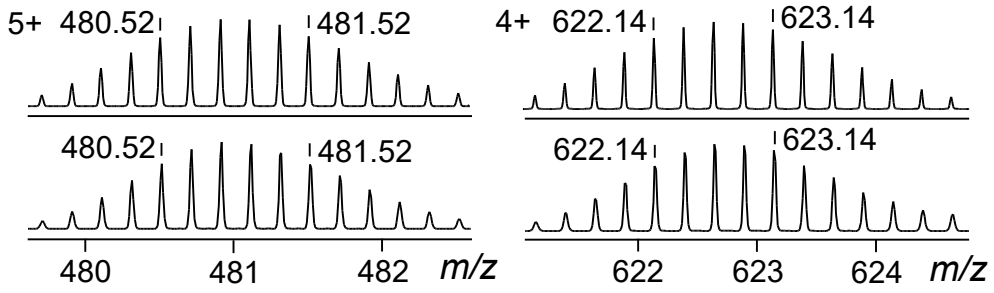

Figure S49. Measured (bottom) and calculated (top) isotope patterns for different charge states observed from $\mathbf{Pd_3L^B_6}$ (BF_4^- as counterion).

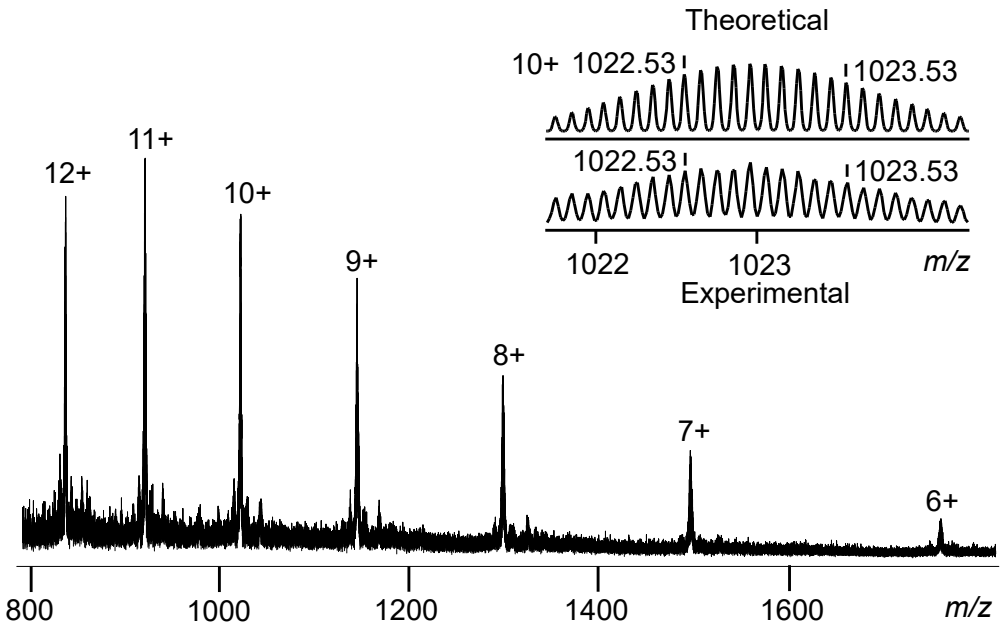

Figure S50. ESI-MS spectrum of cage $\mathbf{Pd_{12}L^{C}_{24}}$ (BF_4^- as counterion).

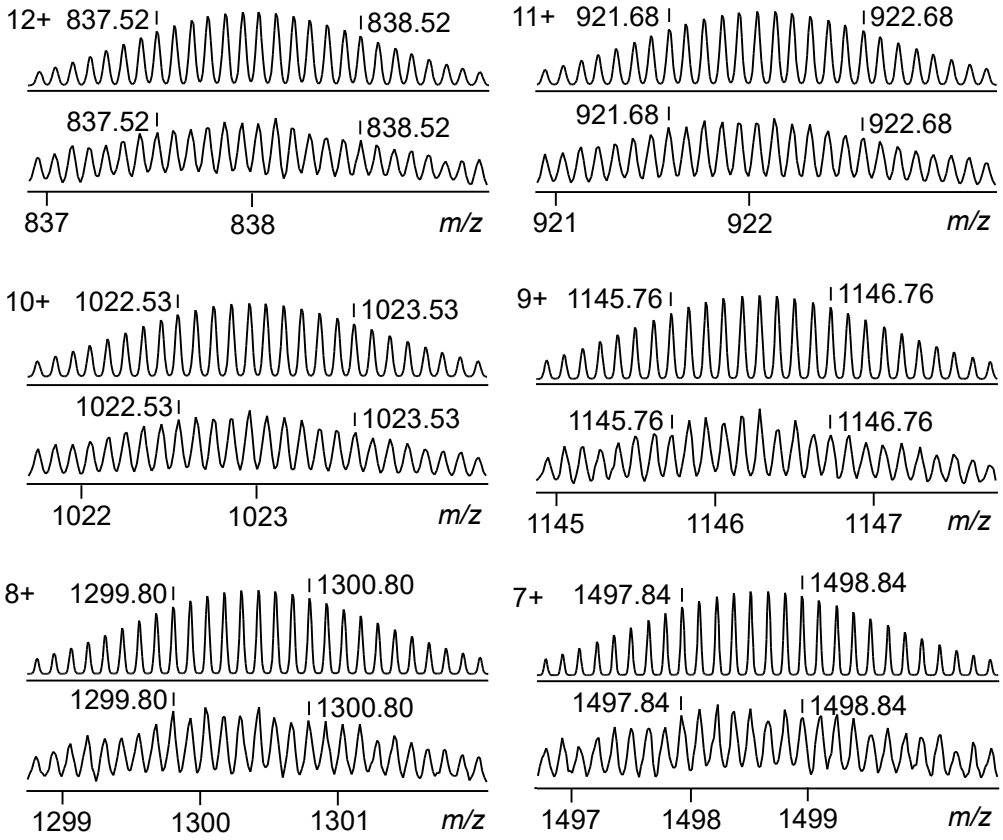

Figure S51. Measured (bottom) and calculated (top) isotope patterns for different charge states observed from $\mathbf{Pd_{12}L^{C}_{24}}$ (BF_4^- as counterion).

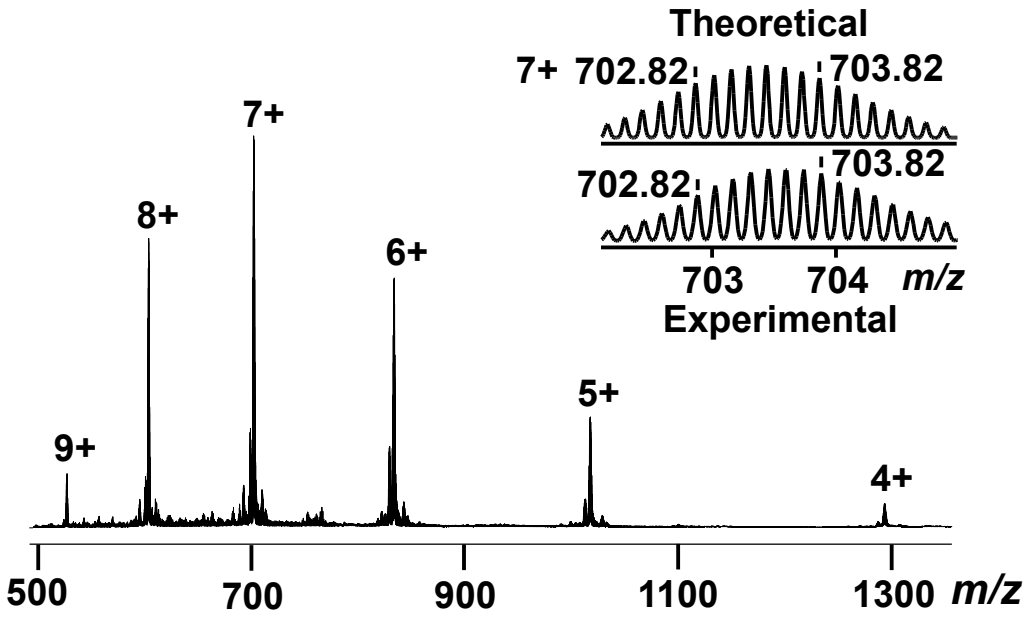

Figure S52. ESI-MS spectrum of $\mathbf{Pd_6L^A{}_6L^B{}_6}$ (BF_4^- as counterion).

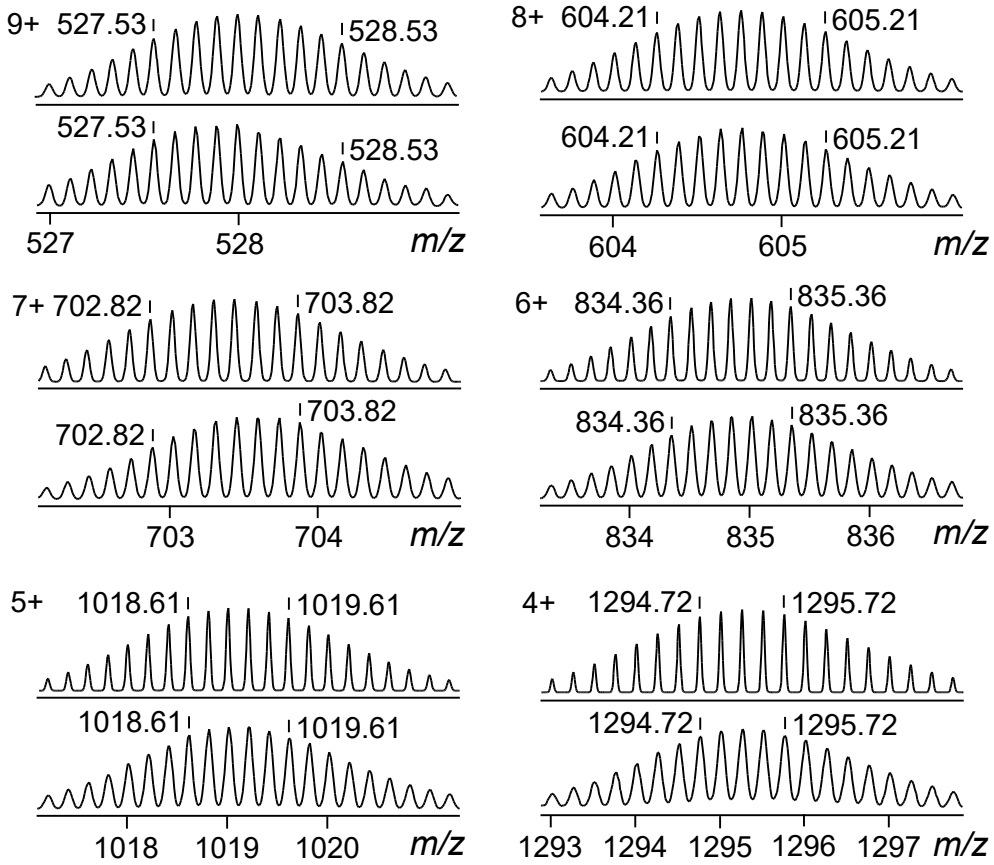

Figure S53. Measured (bottom) and calculated (top) isotope patterns for different charge states observed from $\mathbf{Pd_6L^A{}_6L^B{}_6}$ (BF_4^- as counterion).

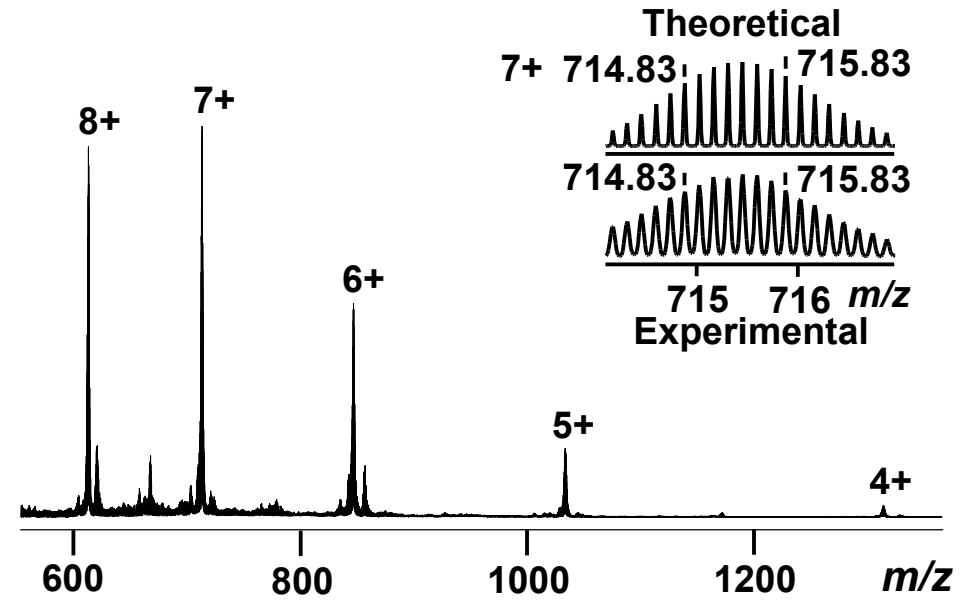

Figure S54. ESI-MS spectrum of $\mathbf{Pd_6L^B_6L^C_6}$ (BF_4^- as counterion).

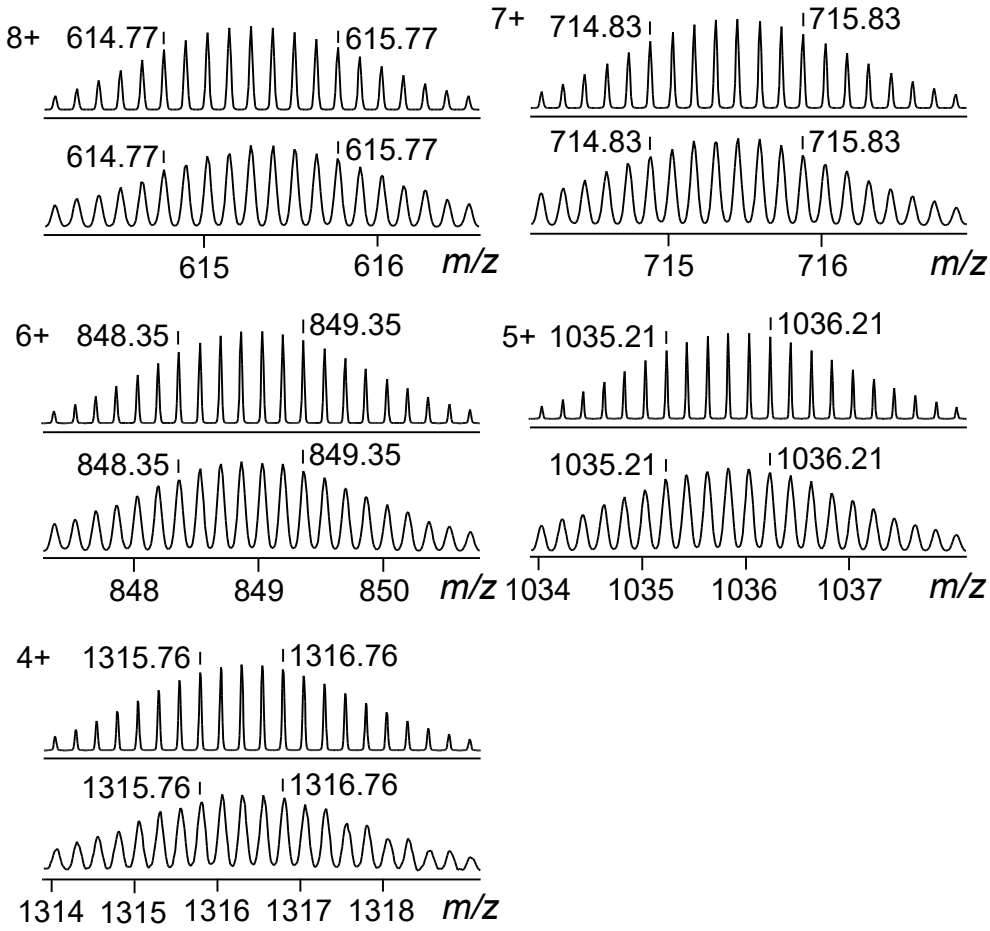

Figure S55. Measured (bottom) and calculated (top) isotope patterns for different charge states observed from $\mathbf{Pd_6L^B_6L^C_6}$ (BF_4^- as counterion).

5. Crystal Information of Complexes

X-ray diffraction data for $\mathbf{Pd_{12}L^{A}_{24}}$, $\mathbf{Pd_6L^{A}_6L^{B}_6}$ and $\mathbf{Pd_6L^{B}_6L^{C}_6}$ were collected using synchrotron radiation and MAR325 CCD detector at Shanghai Synchrotron Radiation BL17B Beamline. Indexing was performed using APEX3.[1] Data integration and reduction was performed using SaintPlus.[2] Absorption correction was performed by multi-scan method implemented in SADABS.[3] Space group was determined using XPREP implemented in APEX3.[1] Structure was solved using SHELXT[4] and was refined using SHELXL-2018[5-6] (full-matrix least-squares on F^2) through OLEX2 interface program.[7] Ellipsoid plot was done with Platon.[8] The refinement of the three crystal structures incorporated restraints and constraints to achieve accurate modeling. Bond distances and angles were restrained to chemically reasonable values, while appropriate restraints on anisotropic displacement parameters ensured model stability and convergence. Partial occupancies were assigned to disordered sites, ensuring the sum remained unity. Geometric similarity restraints were applied to equivalent molecular fragments, and disorder in ligands and metal coordination sites was handled by refining site occupancies and applying thermal restraints. These refinements enhanced the chemical and crystallographic validity of the structures. CCDC: 2387801 [$\mathbf{Pd_{12}L^{A}_{24}}$], 2387551 [$\mathbf{Pd_6L^{A}_6L^{B}_6}$], and 2387553 [$\mathbf{Pd_6L^{B}_6L^{C}_6}$]. ORTEP structures and the unit cell images are shown in ***Figures S56-S61***. Crystal data and refinement conditions are listed in ***Tables S1-S3***.

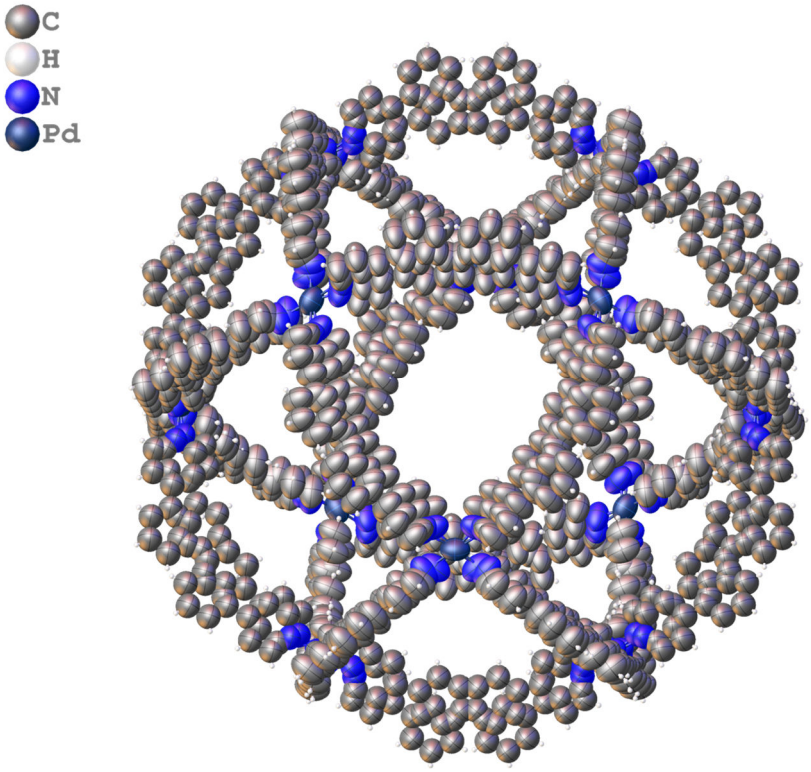

Figure S56. The ORTEP drawing of structure of $\mathbf{Pd_{12}L^{A}_{24}}$.

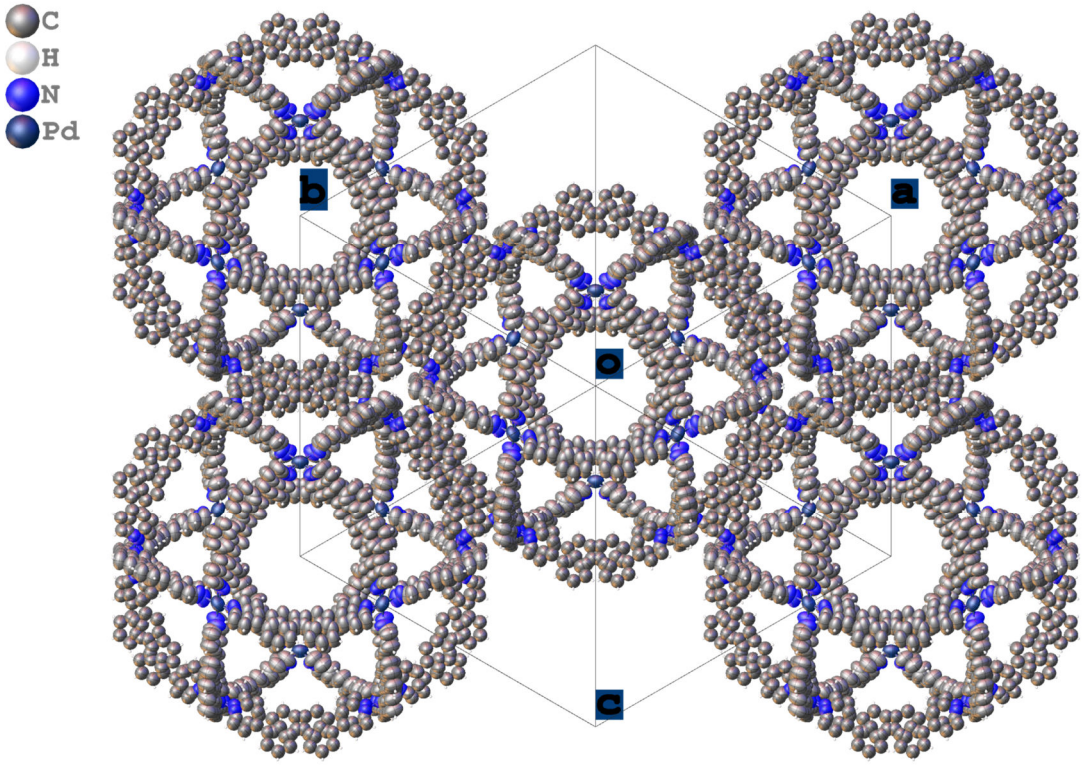

Figure S57. The unit cell packing view from 111 of $\mathbf{Pd_{12}L^{A}_{24}}$.

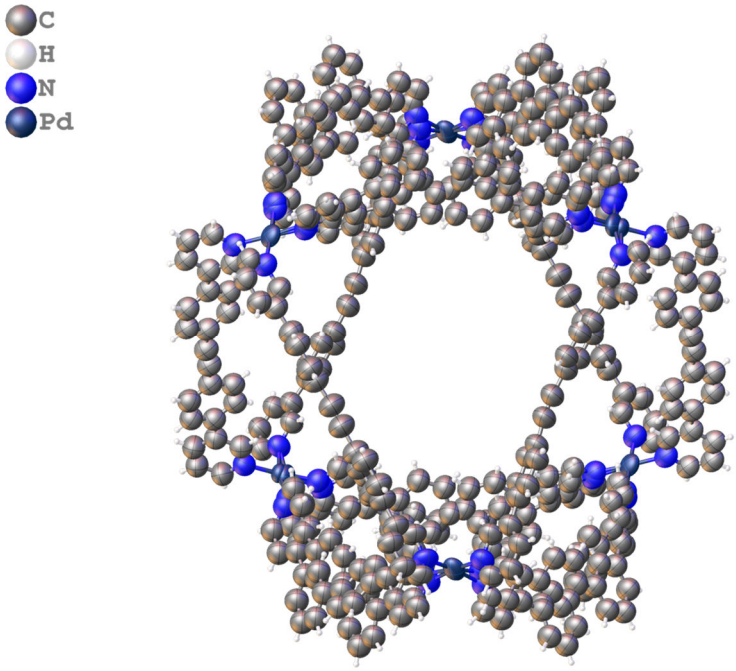

Figure S58. The ORTEP drawing of structure of $\mathbf{Pd_6L^{A}_6L^{B}_6}$.

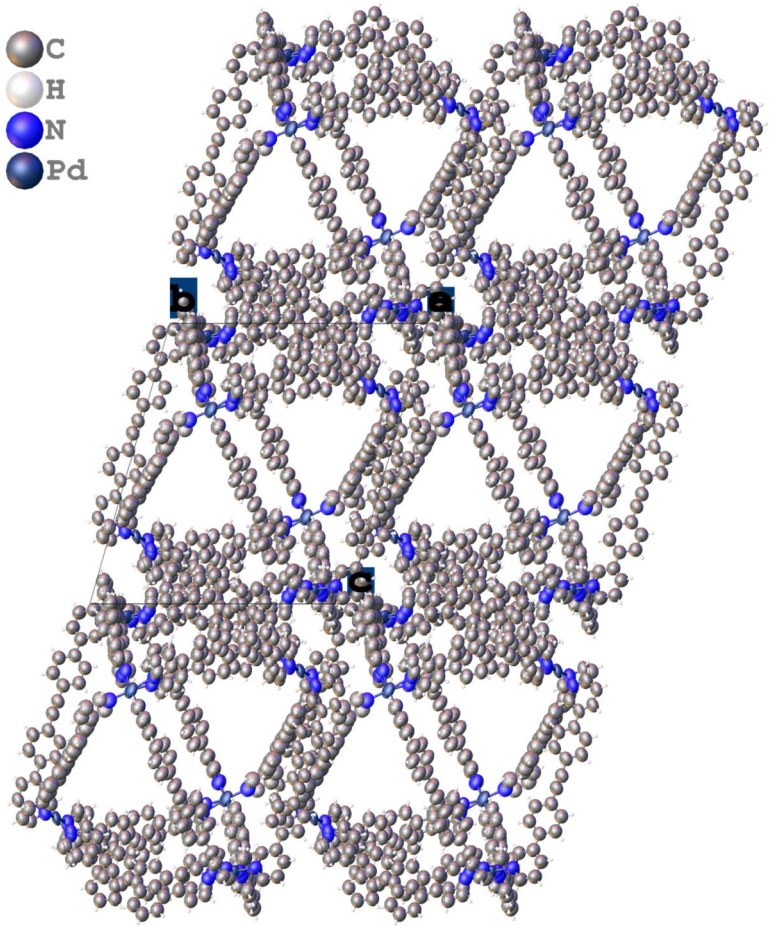

Figure S59. The unit cell packing view from 100 of $\mathbf{Pd_6L^A{}_6L^B{}_6}$.

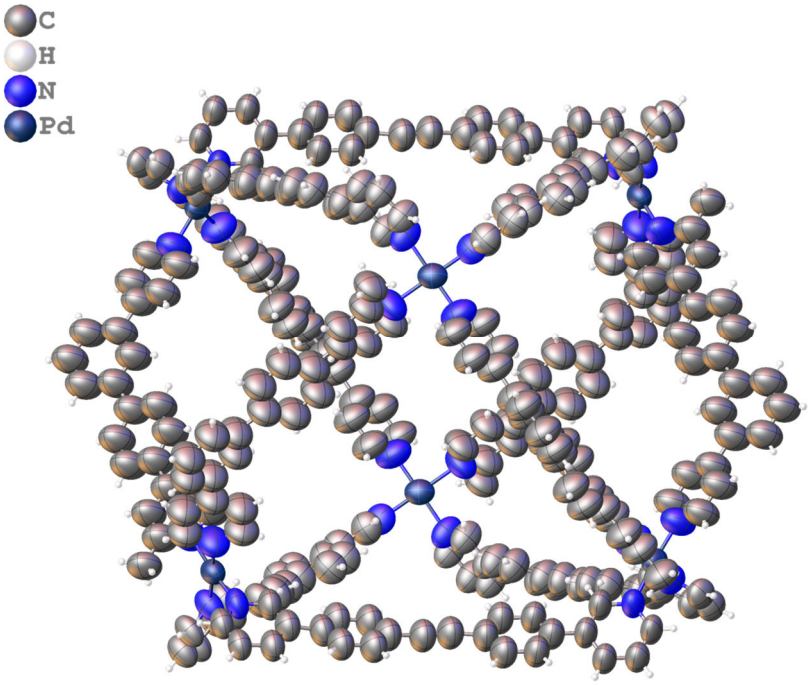

Figure S60. The ORTEP drawing of structure of $\mathbf{Pd_6L^B{}_6L^C{}_6}$.

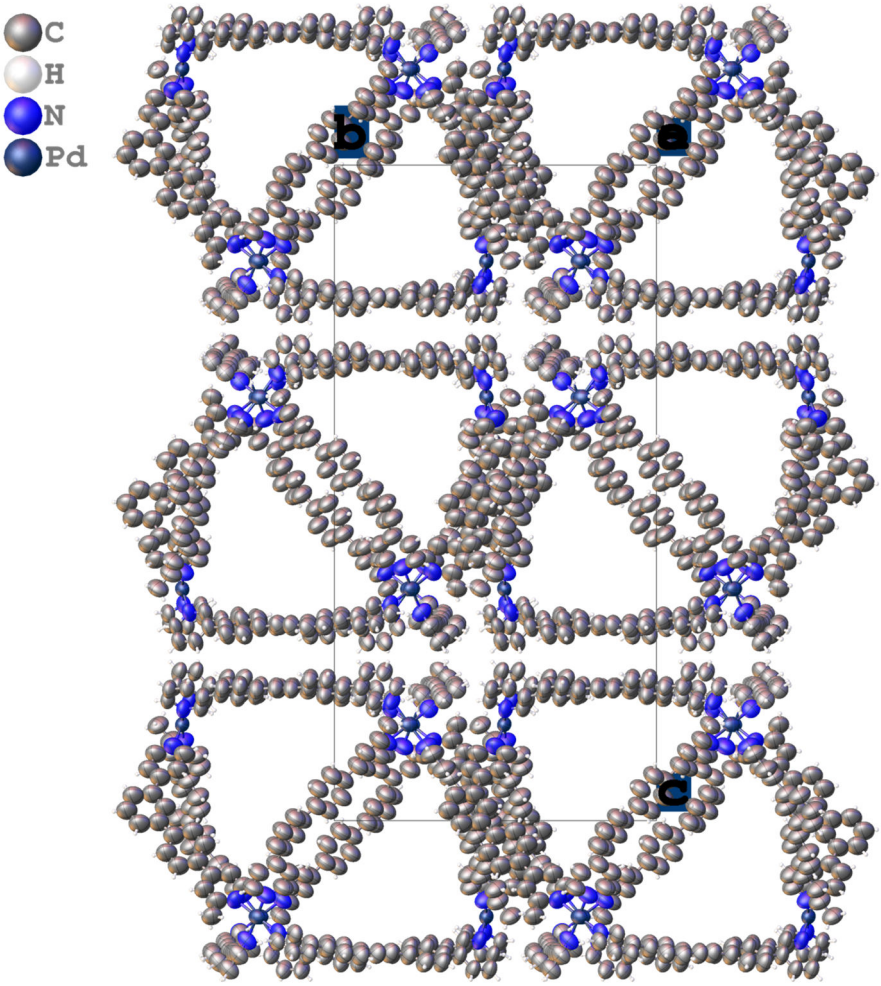

Figure S61. The unit cell packing view from 100 of $\mathbf{Pd_6L^B{}_6L^C{}_6}$.

Table S1. Crystal data and structure refinement for $\mathbf{Pd_{12}L^{A}_{24}}$.

Identification code	$\mathbf{Pd_{12}L^{A}_{24}}$
Empirical formula	$C_{528}H_{384}N_{48}Pd_{12}$
Formula weight	8665.99
Temperature/K	100.00
Crystal system	Cubic
Space group	$Im\bar{3}m$
a/Å	43.650(2)
b/Å	43.650(2)
c/Å	43.650(2)
α/°	90
β/°	90
γ/°	90
Volume/Å^3	83166(12)
Z	6
ρ_{calc}g/cm^3	0.347
μ/mm^{-1}	0.133
F(000)	8880.0
Crystal size/mm^3	0.2 × 0.15 × 0.13
Radiation	Synchrotron (λ = 0.68874)
2Θ range for data collection/°	1.808 to 28.478
Index ranges	-31 ≤ h ≤ 31, -31 ≤ k ≤ 31, -31 ≤ l ≤ 31
Reflections collected	107820
Independent reflections	1525 [R_{int} = 0.0481, R_{sigma} = 0.0099]
Data/restraints/parameters	1525/817/173
Goodness-of-fit on F^2	3.072
Final R indexes [I>=2σ (I)]	R_1 = 0.1787, wR_2 = 0.4941
Final R indexes [all data]	R_1 = 0.1867, wR_2 = 0.5322
Largest diff. peak/hole / e Å^{-3}	1.43/-0.41

Table S2. Crystal data and structure refinement for $\mathbf{Pd_6L^A{}_6L^B{}_6}$.

Identification code	$\mathbf{Pd_6L^A{}_6L^B{}_6}$
Empirical formula	$C_{276}H_{192}N_{24}Pd_6$
Formula weight	4477
Temperature/K	100.00
Crystal system	Triclinic
Space group	$P\bar{1}$
a/Å	24.626(2)
b/Å	24.7677(19)
c/Å	25.970(2)
α/°	69.586(2)
β/°	75.581(2)
γ/°	63.458(2)
Volume/Å^3	13197.9(18)
Z	2
ρ_{calc}g/cm^3	0.564
μ/mm^{-1}	0.195
F(000)	2292.0
Crystal size/mm^3	0.15 × 0.13 × 0.11
Radiation	Synchrotron (λ = 0.67016)
2Θ range for data collection/°	1.954 to 43.674
Index ranges	$-27 \leq h \leq 27$, $-27 \leq k \leq 27$, $-28 \leq l \leq 28$
Reflections collected	124281
Independent reflections	35945 [R_{int} = 0.0551, R_{sigma} = 0.0587]
Data/restraints/parameters	35945/14409/1640
Goodness-of-fit on F^2	1.453
Final R indexes [I>=2σ (I)]	R_1 = 0.1268, wR_2 = 0.3740
Final R indexes [all data]	R_1 = 0.1559, wR_2 = 0.4083
Largest diff. peak/hole / e Å^{-3}	1.54/-0.72

Table S3. Crystal data and structure refinement for $\mathbf{Pd_6L^B_6L^C_6}$.

Identification code	$\mathbf{Pd_6L^B_6L^C_6}$
Empirical formula	$C_{282}H_{204}N_{24}Pd_6$
Formula weight	4561.09
Temperature/K	100.00
Crystal system	Trigonal
Space group	$P\bar{3}1c$
a/Å	26.2350(17)
b/Å	26.2350(17)
c/Å	46.357(4)
α/°	90
β/°	90
γ/°	120
Volume/Å^3	27632(4)
Z	2
ρ_{calc}g/cm^3	0.549
μ/mm^{-1}	0.201
F(000)	4680.0
Crystal size/mm^3	0.15 × 0.12 × 0.1
Radiation	Synchrotron (λ = 0.6887)
2Θ range for data collection/°	1.736 to 32.998
Index ranges	$-21 \le h \le 21$, $-21 \le k \le 21$, $-38 \le l \le 38$
Reflections collected	99021
Independent reflections	5238 [R_{int} = 0.1274, R_{sigma} = 0.1003]
Data/restraints/parameters	5238/1204/374
Goodness-of-fit on F^2	1.397
Final R indexes [I>=2σ (I)]	R_1 = 0.1258, wR_2 = 0.3361
Final R indexes [all data]	R_1 = 0.1399, wR_2 = 0.3594
Largest diff. peak/hole / e Å^{-3}	1.19/-0.34

6. Number of Theoretically Possible Isomers of $Pd_{12}L^{A}_{24}$, $Pd_6L^{A}_6L^{B}_6$-a and $Pd_6L^{A}_6L^{B}_6$-b

6.1 Number of theoretically possible isomers of $\mathbf{Pd_{12}L^{A}_{24}}$.

Referring to the literature published by Fujita et al[9] and Severin et al[10], $\mathbf{Pd_{12}L^{A}_{24}}$ has 700688 isomers in theory. In addition, we can also calculate the same number of isomers by using the mathematical method of Pólya's enumeration theorem[11]. From the analysis of the crystal structure, we can determine that $\mathbf{Pd_{12}L^{A}_{24}}$ are Archimedes tetradecahedron structures, which consist of three pairs of parallel squares and four pairs of parallel triangles, as shown in **Figure S62**. There are 24 sticks in the model, representing the 24 asymmetric ligands in the molecular cage, with the green part representing the short side of the ligand and the yellow part representing the long side. The long and short sides of each ligand can be freely switched between the two metal spheres.

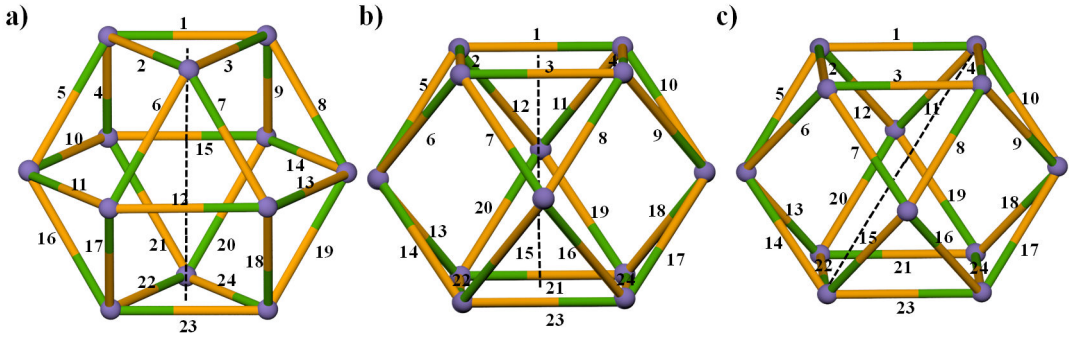

Figure S62. Pictures of three different axis rotations of Archimedes tetradecahedron.

Pólya's enumeration theorem: Let $\bar{G}=\{\overline{P_1}, \overline{P_2}, \ldots, \overline{P_g}\}$ be a permutation group of n objects, and $C(\overline{P_K})$ be the number of cycles permuting $\overline{P_K}$. To color n objects with m colors, the number of coloring schemes is:

$$L = \frac{1}{\bar{G}}\left[m^{C(\overline{P_1})} + m^{C(\overline{P_2})} + \cdots m^{C(\overline{P_g})}\right]$$

(1) Model fixed:

$\overline{P_1}$=（1）（2）（3）（4）（5）（6）（7）（8）（9）（10）（11）（12）（13）（14）（15）（16）（17）（18）（19）（20）（21）（22）（23）（24）

(2) As shown in **Figure S62a**, use the center of two triangles as the axis, number the sides, and rotate the model 120°:

$\overline{P_2}$=（1，2，3）（4，6，8）（5，7，9）（10，12，14）（11，13，15）（16，18，20）（17，19，21）（22，23，24）

There are four pairs of triangles, so there are four kinds of permutation groups, $\overline{P_3}$、$\overline{P_4}$、$\overline{P_5}$ are omitted.

(3) As shown in **Figure S62a**, use the center of two triangles as the axis, and rotate the model 240°:

$\overline{P_6}$=（1，3，2）（4，8，6）（5，9，7）（10，14，12）（11，15，13）（16，20，18）（17，21，19）（22，24，23）

There are four pairs of triangles, so there are four kinds of permutation groups, $\overline{P_7}$、$\overline{P_8}$、$\overline{P_9}$ are omitted.

(4) As shown in **Figure S62b**, use the center of the two squares as the axis, renumber its sides, and rotate the model 90°:

$\overline{P_{10}}$=（1，2，3，4）（5，7，9，11）（6，8，10，12）（13，15，17，19）（14，16，18，20）（21，22，23，24）

There are three pairs of squares, so there are three kinds of permutation groups, $\overline{P_{11}}$、$\overline{P_{12}}$ are omitted.

(5) As shown in **Figure S62b**, use the center of the two squares as the axis, and rotate the model 270°:

$\overline{P_{13}}$=（1，4，3，2）（5，11，9，7）（6，12，10，8）（13，19，17，15）（14，20，18，16）（21，24，23，22）

There are three pairs of squares, so there are three kinds of permutation groups, $\overline{P_{14}}$、$\overline{P_{15}}$ are omitted.

(6) As shown in **Figure S62b**, use the center of the two squares as the axis, and rotate the model 180°:

$\overline{P_{16}}$=（1，3）（2，4）（5，9）（6，10）（7，11）（8，12）（13，17）（14，8）（15，19）（16，20）（21，23）（22，24）

There are three pairs of squares, so there are three kinds of permutation groups, $\overline{P_{17}}$、$\overline{P_{18}}$ are omitted.

(7) As shown in **Figure S62c**, take the line connecting the two oblique vertices as the axis, and rotate the model 180°:

$\overline{P_{19}}$=（1，22）（2，21）（3，24）（4，23）（5，20）（6，19）（7，18）（8，17）（9，16）（10，15）（11，14）（12，13）

There are six kinds of permutation groups in total, removing duplicates, $\overline{P_{20}}$、$\overline{P_{21}}$、$\overline{P_{22}}$、$\overline{P_{23}}$、$\overline{P_{24}}$ are omitted.

C($\overline{P_1}$)=24;

C($\overline{P_2}$)=C($\overline{P_3}$)=C($\overline{P_4}$)=C($\overline{P_5}$)=8;

C($\overline{P_6}$)= C($\overline{P_7}$)=C($\overline{P_8}$)=C($\overline{P_9}$)=8;

C($\overline{P_{10}}$)=C($\overline{P_{11}}$)=C($\overline{P_{12}}$)=6;

C($\overline{P_{13}}$)=C($\overline{P_{14}}$)=C($\overline{P_{15}}$)=6;

C($\overline{P_{16}}$)=C($\overline{P_{17}}$)=C($\overline{P_{18}}$)=12;

C($\overline{P_{19}}$)=C($\overline{P_{20}}$)=C($\overline{P_{21}}$)= C($\overline{P_{22}}$)=C($\overline{P_{23}}$)=C($\overline{P_{24}}$)=12

In summary: permutation groups $\overline{G}$=1+4+4+3+3+3+6=24，L=（2^{24}+4*2^{8}+4*2^{8}+3*2^{6}+3*2^{6}+3*2^{12}+6*2^{12}）/24=700688, that is, Archimedes tetradecahedron model corresponding to **$Pd_{12}L^{A}_{24}$** has 700688 substantially different structures, which means that the number of isomers in **$Pd_{12}L^{A}_{24}$** theoretically is 700688.

6.2 Number of theoretically possible isomers of **$Pd_6L^{A}_6L^{B}_6$-a** and **$Pd_6L^{A}_6L^{B}_6$-b**.

In **$Pd_6L^{A}_6L^{B}_6$-a** and **$Pd_6L^{A}_6L^{B}_6$-b**, each of the six asymmetric ligands can adopt two orientations, theoretically leading to 2^6 = 64 isomers (including duplicates). Compared to the complex isomer count of the **$Pd_{12}L^{A}_{24}$** cage, the isomer calculation for **$Pd_6L^{A}_6L^{B}_6$-a** and **$Pd_6L^{A}_6L^{B}_6$-b** is more manageable. Using an enumeration method to eliminate duplicates, we identified 16 isomers for **$Pd_6L^{A}_6L^{B}_6$-b** (Figure S63) and 13 isomers for **$Pd_6L^{A}_6L^{B}_6$-a** (Figure S64).

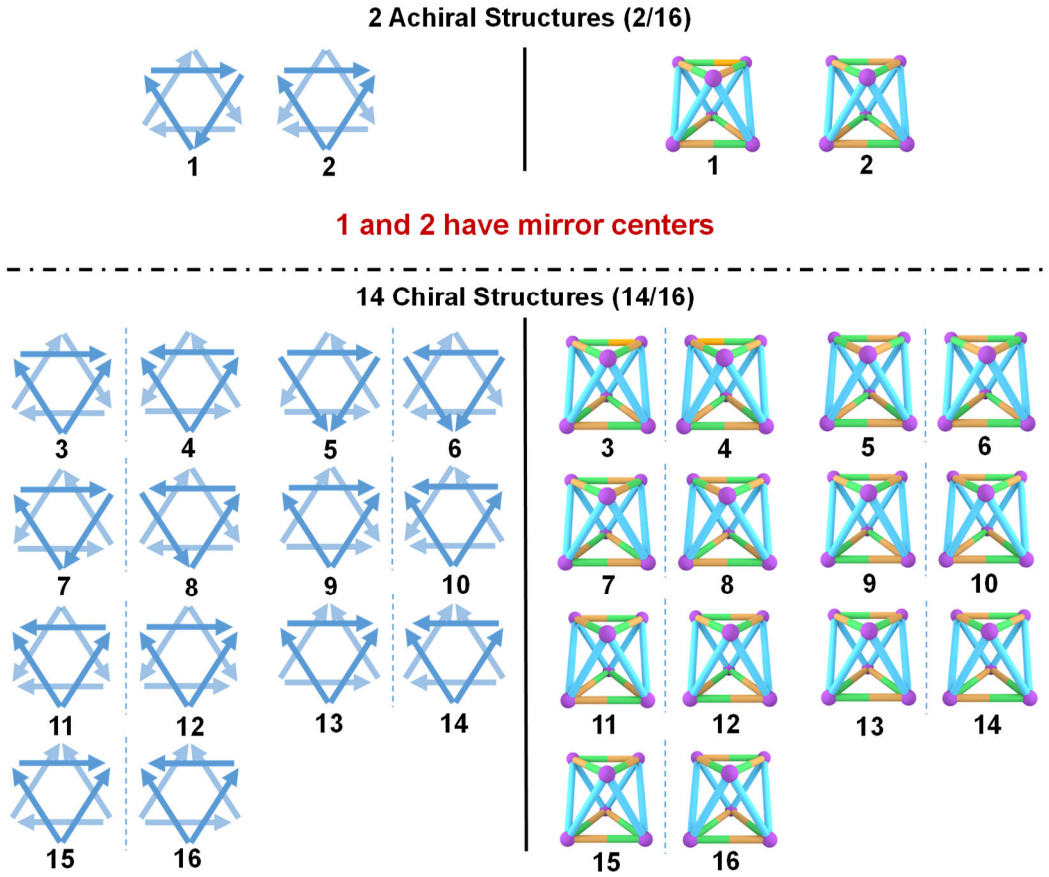

Figure S63. Sixteen potential configurations of **$Pd_6L^{A}_6L^{B}_6$-b**.

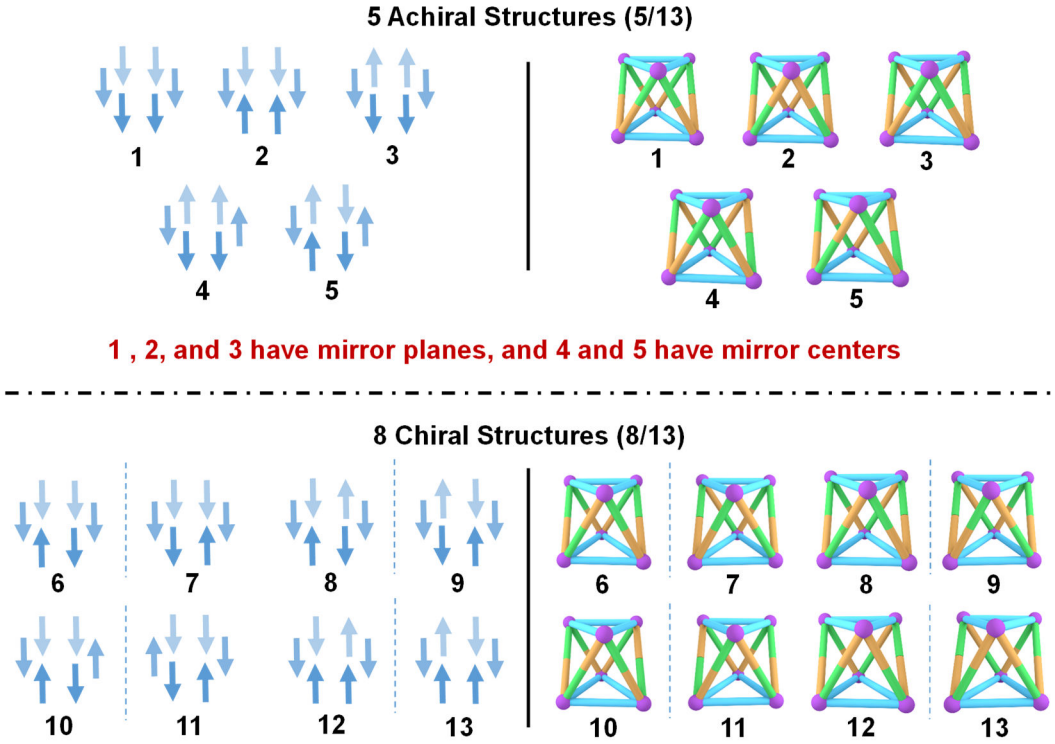

Figure S64. Thirteen potential configurations of $\mathbf{Pd_6L^A{}_6L^B{}_6}$**-a**.

7. Density Functional Theory Calculations

The calculations of the six binding modes of Pd^{2+} and ligands in $[\mathbf{Pd_{12}L^{C}_{24}}]^{24+}$ were performed using Gaussian 16 software, and the PBE0 function was used at the DFT level. A mixed basis set was used in the calculations, including the effective core potential Lanl2dz for Pd^{2+} and 6-31G for other atoms. The geometry is fully optimized without any structural constraints. Numerical frequency calculations were performed at the same level to confirm the stable geometry.

There are six coordination modes for the interaction between $\mathbf{L^{C}}$ and Pd(II) (**Figure S65**), namely **LLLL**, **SSSS**, **LSLS**, **LLSS**, **LLLS**, and **LSSS**. The calculation results indicate that the **LSLS** coordination mode has the highest binding energy. This suggests that in $\mathbf{Pd_{12}L^{C}_{24}}$, Pd(II) centers are more likely to form coordination modes in which the ligands are connected in *trans*, because this coordination mode can form the most stable structure. Therefore, we infer that the complex of $\mathbf{L^{C}}$ has a single configuration, which is ***trans*-$\mathbf{Pd_{12}L^{C}_{24}}$** (**Figure S66**).

The binding energy for each coordination mode is calculated as follows:

$E_b = E_{Complexes} - (n \times E_{Ligand} + E_{Metal\text{-}ion})$

$E_{Complexes}$: total energy of a coordination mode;

E_{Ligand}: energy of ligand;

$E_{Metal\text{-}ion}$: energy of metal Pd(II);

n: number of ligands;

E_b: binding energy of Pd(II) and ligand.

LLLL: E_{b1} = -4107.971144 - (4×-995.393793-125.54493) = -534.028855 kcal/mol

SSSS: E_{b2} = -4107.974864 - (4×-995.393793-125.54493) = -536.363155 kcal/mol

LSLS: E_{b3} = -4107.975238 - (4×-995.393793-125.54493) = -536.59784 kcal/mol

LLSS: E_{b4} = -4107.974081 - (4×-995.393793-125.54493) = -535.8718225 kcal/mol

LLLS: E_{b5} = -4107.9731 - (4×-995.393793-125.54493) = -535.256245 kcal/mol

LSSS: E_{b6} = -4107.975042 - (4×-995.393793-125.54493) = -536.47485 kcal/mol

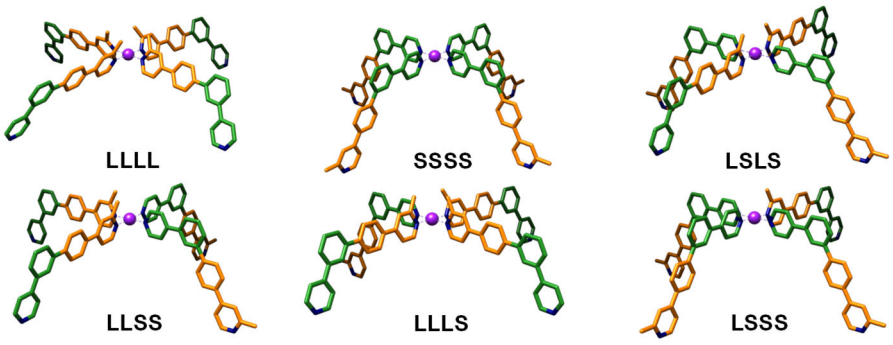

Figure S65. Six binding modes of $\mathbf{L^{C}}$ and Pd(II) in $\mathbf{Pd_{12}L^{C}_{24}}$.

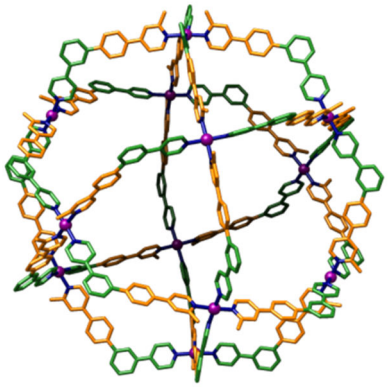

Figure S66. Structural simulation of ***trans*-$Pd_{12}L^{C}_{24}$**.

8. Reference

[1] Bruker (2018.7-2). *APEX3*. Bruker AXS Inc., Madison, Wisconsin, USA.

[2] Bruker (2018) SAINT. Data Reduction Software.

[3] Sheldrick, G. M. (1996). SADABS. *Program for Empirical Absorption Correction.* University of Gottingen, Germany.

[4] Sheldrick, G. M. *Acta Cryst.* (2015). A71, 3-8.

[5] Sheldrick, G. M. *Acta Cryst.* (2008). A64, 112-122.

[6] Sheldrick, G. M. *Acta Cryst.* (2015). C71, 3–8.

[7] Dolomanov, O.V.; Bourhis, L.J.; Gildea, R.J.; Howard, J.A.K.; Puschmann, H. OLEX2: A complete structure solution, refinement and analysis program. *J. Appl. Cryst.*, **2009**, *42*, 339-341.

[8] A.L.Spek, Single-crystal structure validation with the program PLATON. *J. Appl. Cryst*. **2003**, *36*, 7-11.

[9] Sun, Q.F.; Sato, S.; Fujita, M. An $M_{12}(L1)_{12}(L2)_{12}$ cantellated tetrahedron: a case study on mixed-ligand self-assembly. *Angew. Chem. Int. Ed.* **2014**, 53, 13510–13513

[10] Li, R.J.; Tarzia, A; Posligua, V; Jelfs, K.E; Sanchez, N; Marcus, A; Baksi, A; Clever, G.H; Fadaei-Tirani, F; Severin, K. Orientational self-sorting in cuboctahedral Pd cages. *Chem. Sci.,* **2022,** 13, 11912–11917.

[11] G. Pólya; R. C. Read (1987). Combinatorial Enumeration of Groups, Graphs, and Chemical Compounds. ISBN 0-387-96413-4.